Meteorological Impacts of Offshore Wind Turbines as Simulated in the Weather Research and Forecasting Model

Daphne Quint[1,2], Julie K. Lundquist[1,2,3,4], Nicola Bodini[2], and David Rosencrans[1]

[1]Department of Atmospheric and Oceanic Sciences, University of Colorado Boulder, Boulder, Colorado, 80309-0311, United States
[2]National Renewable Energy Laboratory, Golden, Colorado, 80401, United States
[3]Renewable and Sustainable Energy Institute, Boulder, Colorado, 80309, United States
[4]Johns Hopkins University, Baltimore, Maryland, 21218, United States

Correspondence: Nicola Bodini (nicola.bodini@nrel.gov)

Abstract. Offshore wind energy projects are currently in development off the east coast of the United States and ~~will likely~~ may influence the local meteorology of the region. Wind power production and other commercial uses in this area are related to atmospheric conditions, and so it is important to understand how future wind plants will change the local meteorology. We compared one year of simulations from the Weather Research and Forecasting model with and without wind farms incorporated, focusing on the lease area south of Massachusetts and Rhode Island. We assessed changes in wind speeds, 2 m temperature, surface heat flux, turbulent kinetic energy, and boundary layer height during different stability classifications and ambient wind speeds over the entire year. Because the wake behavior may be a function of boundary-layer stability, in this paper, we also present a machine learning algorithm to quantify the area and distance of the wake generated by the wind plant. This analysis enables us to identify the relationship between wake extent and boundary-layer height. ~~Hub-height~~ We find that hub-height wind speed is reduced within and downwind of the wind plant, with the strongest impacts occurring during stable conditions and faster wind speeds in region 3 of the turbine power curve, although impacts lessen as wind speeds increase past 15 m s^{-1}. Wind speeds at 10 m increase within the wind plant area during stable conditions, and this increase persists as wind speed increases. Differences in 2 m temperatures and surface heat fluxes are small, but are largest during stable conditions and ~~strong~~ fast wind speeds. Turbulence kinetic energy (TKE) increases within the lease area with increasing wind speeds at both the surface and at hub height. At hub height, TKE increases do not depend on stability, but at the surface, TKE increases most during unstable conditions as the turbulence injected at hub height is mixed down to the surface. Boundary-layer heights increase within the wind plant, and decrease slightly downwind during stable conditions. ~~Deeper~~ Shallower boundary-layer heights ~~, exceeding 100 m,~~ tend to correlate with ~~smaller~~ larger wake areas and distances, though other factors likely also play a role in determining the extent of the wind farm wake.

Copyright statement. This work was authored in part by the National Renewable Energy Laboratory, operated by Alliance for Sustainable Energy, LLC, for the U.S. Department of Energy (DOE) under contract no. DE-AC36-08GO28308. Funding was provided by the U.S. Department of Energy Office of Energy Efficiency and Renewable Energy Wind Energy Technologies Office. The views expressed in the

1 Introduction

Wind plants along the northeastern U.S. coast are projected to undergo rapid expansion in the coming years, aiming to achieve a capacity of 30 GW by 2030 and 110 GW by 2050 (U.S. Department of Energy, 2023). Currently, 27 areas are leased along the mid-Atlantic Outer Continental Shelf for future offshore wind development (Bureau of Ocean Energy Management, 2023). Wind plants produce wakes that can influence local environments. Only a limited set of observations have quantified the effects of wind plants on local meteorology, and so a combination of observational and modeling studies have been used to assess micrometeorological impacts of wakes.

The aggregation of individual wind turbine wakes into a wind farm wake results in a wind speed deficit downwind of the wind plant (Christiansen and Hasager, 2005; Platis et al., 2018, 2020), with the strongest deficit generally occurring in the top half of the turbine rotor disk (Bodini et al., 2021). Stronger and larger wakes are also associated with stable conditions, moderate wind speeds, low boundary-layer heights, and low ambient turbulence kinetic energy (TKE) (Christiansen and Hasager, 2005; Dörenkämper et al., 2015; Platis et al., 2018; Lundquist et al., 2019; Fischereit et al., 2022a; Pryor et al., 2021; Bodini et al., 2021; Rosencrans et al., 2024). TKE is enhanced near wind plants, but this increase diminishes rapidly downwind (Bodini et al., 2021). The most pronounced enhancement in TKE typically occurs in the upper half of the turbine rotor disk. The degree of TKE increase is influenced by atmospheric stability: in unstable conditions, ambient TKE levels are high, resulting in only a slight increase in TKE in the presence of wind plants; in contrast, during stable conditions, wind plants significantly increase TKE levels (Bodini et al., 2021).

Wind farms can also cause changes in surface temperatures. Wind plants tend to cause a warming at the surface during stable conditions (Baidya Roy and Traiteur, 2010; Fitch et al., 2013; Rajewski et al., 2014; Siedersleben et al., 2018a; Golbazi et al., 2022). The hypothesis proposed by Baidya Roy and Traiteur (2010) suggests that enhanced vertical mixing induced by wind turbine wakes causes this warming. During stable conditions, temperature increases with height, so enhanced mixing at the surface would result in warmer air from aloft mixing with cooler air at the surface. Similarly, during unstable conditions, cooler air from aloft is mixed with surface air, resulting in a cooling effect. This warming effect in stable conditions has been observed in wind farms near peat bogs in Scotland (Armstrong et al., 2016), wind farms in cropland in Iowa (Rajewski et al., 2014), a wind farm in farmland/grassland in China (Luo et al., 2021), and other locations. Satellite observations also suggest apparent surface warming due to the mixing of warm air down to the surface in stably stratified conditions ~~Zhou et al. (2012b, a); Walsh-Thomas et al. (2012); Harris et al. (2014); Slawsky et al. (2015); Xia et al. (2016); Chang et al. (2016)~~ (Zhou et al., 2012b, a; Walsh-Thomas et al., 2012; Harris et al., 2014; Slawsky et al., 2015; Xia et al., 2016; Chang et al., 2016) . In contrast, the VERTEX field campaign, in coastal marshland, did not find increased TKE or momentum fluxes in comparison to non-waked areas, suggesting that vertical mixing is not responsible for the observed temperature changes (Archer et al.,

2019). The exact nature of the wind farm warming effect is likely due to complex interactions between the ambient atmosphere, the wind turbine wake, and surface characteristics.

The height of the wind turbine can also ~~influences~~ influence temperature changes in the wind plant. Golbazi et al. (2022) compared surface temperature changes for turbines with a hub height of 81 m to ~~"extreme-scale"~~ turbines with hub heights
of 119 m and 250 m. Warming was observed below the turbine for both cases; however, for the ~~extreme-scale turbines~~ bigger turbines in this study, warming did not extend all the way to the surface. Instead, slight cooling was found at the surface.

Changes in surface temperatures are coupled with heat flux changes at the surface. When conditions are unstable, heat fluxes are typically positive (upward). Similarly, during stable conditions when warmer air lies over cooler air, heat fluxes are negative (downward) (Stull, 1988). According to Golbazi et al. (2022), the magnitude of the heat flux decreases in areas experiencing cooling. This weakening is indicated by a positive change when the atmosphere is stable and a negative change when the atmosphere is unstable. As part of the Crop Wind-Energy Experiment campaign, Rajewski et al. (2014) found that turbines have the largest influence on surface heat flux at night, in which a larger transport of heat was observed as warm air from aloft was brought to the surface by turbine-induced mixing. In contrast, during the day, the turbine-induced mixing was weaker than the ambient boundary-layer-scale mixing, resulting in inconsistent signals of warming and cooling differences between times with and without turbines. The large-eddy simulations of Lu and Porté-Agel (2011) also find that turbines induce strong changes on heat and momentum fluxes in a stable boundary layer.

In some circumstance, wind turbines effects can also influence a deeper region of the atmosphere. The planetary boundary layer height (PBLH) is the height of the layer of the atmosphere that is influenced by the surface. Wind plants increase the boundary-layer height in stable (Lu and Porté-Agel, 2011) and neutral (Wu and Porté-Agel, 2017) conditions. As wind turbines extract energy from incoming flow, kinetic energy is entrained from the flow above, resulting in an increased boundary layer depth. An internal boundary layer (IBL) develops above the wind plant as relatively slower flow at rotor height moves upwards, interacting with slightly faster air. The IBL grows; it may eventually interact with the free atmosphere and modify the planetary boundary layer (PBL) height (Wu and Porté-Agel, 2017; Gadde and Stevens, 2021). The growth of the IBL is dependent on the stratification of the boundary layer with which it interacts. During situations with weak stratification in the free atmosphere above the PBL, the IBL can nudge the PBL to deeper heights. However, when the layer above the PBL is strongly stratified, the IBL cannot necessarily push the PBL higher (Wu and Porté-Agel, 2017). Because the vertical growth of the boundary layer is limited for these strongly stratified conditions, flow instead goes around the wind plant in the horizontal direction (Gadde and Stevens, 2021).

The relationship of the boundary-layer height with wake length is also an area of active research. Weather Research and Forecasting (WRF) model simulations of Pryor et al. (2021) in this region found that lower PBL heights favor longer and more intense wakes, though stable conditions and low ambient TKE also increase wake strength and extent. In the German bight, the large-eddy simulations of Maas and Raasch (2022) also find longer wakes for shallower boundary layers, with some wakes exceeding 100 km.

~~In this paper, we aim to determine how~~ Given the scarcity of comprehensive offshore observations along the U.S. East Coast, this study aims to complete the first year-long assessment of how modeled offshore wind plants influence the ~~local~~

~~environment~~ modeled local environment. We achieve this by comparing WRF model (Skamarock et al., 2021) simulations with and without wind plants included~~over a one-year period. We~~. Our analysis focuses on the Massachusetts-Rhode Island offshore wind lease area, where we quantify the difference in hub-height and ~~10 m~~ 10-m wind speed, boundary-layer height, ~~2 m~~ 2-m temperature, surface heat flux, and TKE at the surface and at hub height~~in the Massachusetts-Rhode Island offshore wind lease area. We compare differences between simulations for different stability classifications and ambient wind speeds. Finally, we~~ Our expectation is to demonstrate that different stability conditions are a key driver of the simulated micrometeorological impacts, and that these impacts also vary with different wind speeds, as wind turbine operation changes. Furthermore, we aim to assess the relationship between ~~the~~ boundary-layer height and the ~~extension of the~~ extent of wind plant wakes, hypothesizing that deeper boundary layers will limit the extension of these wakes. In Sect. 2, we describe the dataset used for our analysis, and in Sect. 3 we introduce our method to determine the extension of the wakes using machine learning. We present our results in Sect. 4 and provide conclusions and suggested future work in Sect. 5.

2 Dataset

In this study, we use the NOW-WAKES dataset introduced in Rosencrans et al. (2024) as part of the 2023 National Offshore Wind dataset (Bodini et al., 2024b). Full details on the dataset can be found in Rosencrans et al. (2024), but a brief summary is provided here. We note that the WRF setup used here resulted from a comparison of 16 different WRF setups against an observational dataset (Bodini et al., 2024b); this setup was the best performer. The dataset was created using WRF version 4.2.1, and the wind plant parameterization of Fitch et al. (2012) updated with the bug fix of Archer et al. (2020) but with 100 % added TKE rather than 25 % added TKE. We use the innermost domain (domain 2) of the two nested domains, bounded by 76.208W - 64.977W and 37.389N - 42.137N (Figure 1). Domain 2 has a 2 km horizontal resolution and a 10m vertical resolution near the surface with stretching aloft. There were 34 vertical levels in the lowest 2,000 m, and 29 in the lowest 750 m. ~~The period~~ NOW-WAKES covers from 1 September 2019 00:00 UTC - 31 August 2020 23:50 UTC ~~provides a temporal resolutionof 10 minutes~~(chosen to overlap with lidar data availability in the region) at 10-minute resolution; we used hourly time steps for our analysis. The Rosencrans et al. (2024) domain is consistent with other datasets for this region (Xia et al., 2022; Redfern et al., 2023; Bodini et al., 2024b) and was initially chosen to optimize processor partitioning for the WRF simulations.

We consider two sets of NOW-WAKES simulations (Table 1). The first simulation ("no wind farm", NWF) does not include any wind turbines, and has been validated in comparison to floating lidar observations at two locations in the domain (Rosencrans et al., 2024). The other simulation considers a wind turbine layout with turbines from all lease areas (LA100). For this analysis, we compare the NWF simulation to the LA100 simulation, as this layout is most relevant for the region of interest marked in Figure 1. (The "100" refers to the 100 % added TKE factor.) Figure 1 shows the locations of the wind turbines for each of these simulations. The turbines introduced in these simulations are 12 MW with a rotor disk extending from 30 m to 245 m and a hub-height of 138 m. The power~~curve~~, thrust coefficient, and power coefficient curves for these turbines ~~is described by~~ appear in Figure 2. To assess the effect of including turbine-generated TKE, separate simulations with 0 % and

100 % added TKE are available, but we consider only the 100 % TKE simulation as comparisons to large-eddy simulations.

(Vanderwende et al., 2016) Vanderwende et al. (2016) suggest that added TKE is critical. ~~When~~ In that study, when TKE generation within the wind farm parameterization is disabled, the model produced unrealistic wind speeds, wind directions, and turbulence as compared to large-eddy simulations, with too-small of values of turbulence and too large of decreases in wind speed.

The topic of how much turbine-generated turbulence to incorporate into mesoscale wind farm parameterizations is an active area of research. The initial default value recommended by Fitch et al. (2012) was 100 %. In later work, Archer et al. (2020) recommended a value of 25 % based on their large-eddy simulations of an individual turbine in neutrally-stratified simulations. More recent comparison with field observations, using the bug fix and corrected TKE advection (Larsén and Fischereit, 2021; Ali et al., 202 both suggest that 100 % added TKE yields better agreement with observations. Given this uncertainty in the literature and the experience of the sensitivity study of Rosencrans et al. (2024) (their Supplemental Figure A1b and d) that the amount of added TKE makes a very subtle impact on surface fluxes, we return to the original default value of 100 % added TKE for these simulations.

Table 1. Summary of the two NOW-WAKES simulations considered in our analysis.

Simulation Type	Acronym	Turbine Type	Time Period	Added TKE	# Turbines
No wind plants	NWF	N/A	09/01/2019 - 08/31/2020	N/A	0
All lease areas	LA100	12 MW	09/01/2019 - 08/31/2020	100%	1418

2.1 Quantities of interest

We focus on assessing the impact of offshore wind turbines on wind speed, 2 m temperature, surface heat flux, TKE (modeled in WRF as QKE, or twice the TKE), and planetary boundary layer height. Figures of average hub-height wind speed, 10 m wind speed, 2 m temperature, surface ~~QKE~~TKE, and sea-surface temperature in each season are available in the appendix (Figs. A1, A2, A3, A4 and A5). All other quantities are discussed in further detail here.

We assess the impact of wind plants on surface heat flux. Positive surface heat flux values refer to the transfer of heat upwards, which is common during unstable conditions when warmer air underlies cooler air. Negative surface heat flux values are common in stable conditions, and refer to the transfer of heat downwards. Heat flux varies seasonally and by location (Fig. 3). In spring and summer over water, heat fluxes are often negative due to the more frequent occurrences of stable conditions. Heat fluxes are also relatively consistent across the region. In fall and winter, heat fluxes are positive due to more frequent unstable stratification. Heat fluxes during these months vary with distance from the coast, becoming more strongly positive further from the coast.

We also consider how wind plants influence turbulence at hub height and at the surface. WRF outputs QKE, which is defined as 2 times the TKE, and is the relevant variable from the Mellor–Yamada– Nakanishi–Niino (MYNN) PBL scheme used here.
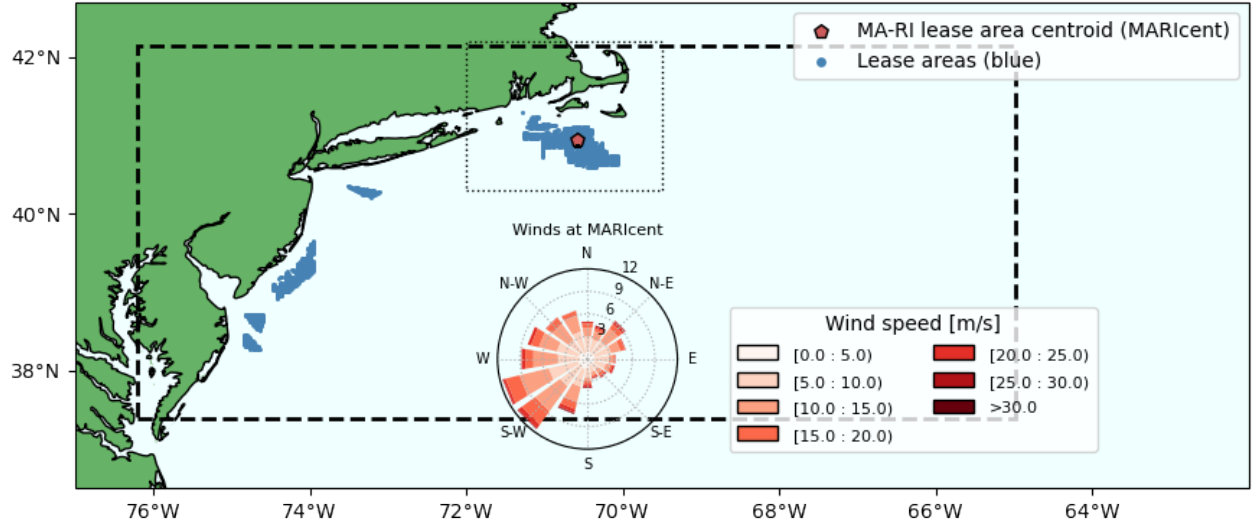
Figure 1. Simulation domain, including turbine locations and a wind rose near the centroid of the Massachusetts-Rhode Island lease area (MARIcent). The MARIcent location is marked in red. The turbine locations are shaded, and all wind plants included in the lease area simulations are in blue. The boundary of the NOW-WAKES innermost domain is outlined in the dashed black line. The dotted gray line indicates the region of interest for this study. The wind rose shows the wind speed (shading) and direction (angle) at 130 m over the 1 year modeled in NOW-WAKES. The distance from the center of the rose indicates the percentage of values in each bin.
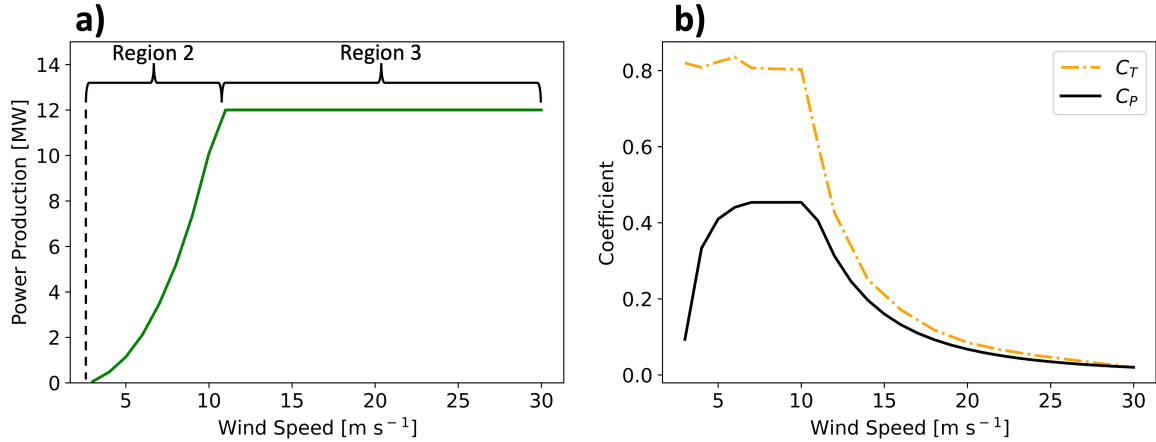
Figure 2. Characteristics of the 12-MW turbine used in the NOW-WAKES simulations. (a) The power curve and (b) curves showing the thrust coefficient (C_T) in dashed orange and power coefficient (C_P) in solid black. Figure courtesy of Rosencrans et al. (2024).

In the MYNN PBL scheme, TKE created by sub-grid processes such as wind plants is not always advected horizontally, but TKE advection (Archer et al., 2020) is turned on in these simulations (Rosencrans et al., 2024). TKE estimates the intensity
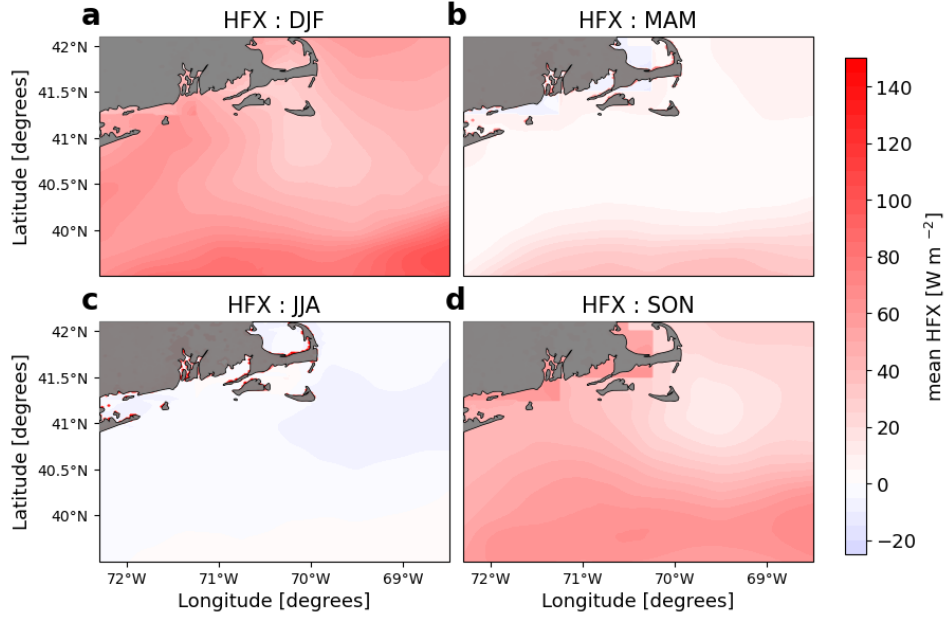
Figure 3. ~~Same as in Fig. 5, but for~~ Average surface heat flux in the region from the NWF simulation is shown for each season from September 2019 – August 2020. (a) December, January and February (DJF) (b) March, April, and May (MAM) (c) June, July, and August (JJA) (d) September, October, and November (SON).

of turbulence and is produced mechanically by wind shear or by buoyant thermals. The change in TKE over time depends on advection, shear generation, buoyant production, ~~self transport, wind turbine production,~~ turbulent transport, and the viscous

155 dissipation rate (Nakanishi and Niino, 2009), and, in the LA100 simulations here, production due to wind turbine motion. Hub-height ~~QKE~~ TKE varies seasonally and by location (Fig. 4). In the spring and summer, ~~QKE~~ TKE at hub height is small due to the prevalence of stable conditions. In the fall and winter, ~~QKE~~ TKE is larger due to more frequent unstable conditions. ~~QKE~~ TKE increases with distance from the coast, especially during the fall and winter.

Wind turbines generally operate within the boundary layer, and thus may influence ~~the PBLH~~and be influenced by the height

160 of the PBL. Deeper planetary boundary layer (PBL) heights are associated with faster wake recovery due to the larger volume of air that can be drawn into the wake (Maas and Raasch, 2022; Pryor and Barthelmie, 2024). In the MYNN PBL scheme used in the NOW-WAKES WRF simulations, the PBLH is derived from a blend of a potential temperature and TKE-based definitions, depending on the stability of the atmosphere (Olson et al., 2019). For stable conditions, most relevant for significant wakes, the TKE definition dominates, and the boundary layer height is the height at which turbulent motions drop to 5% of the surface

165 TKE value (Olson et al., 2019). During neutral and unstable conditions, the potential temperature definition dominates, and the boundary-layer height is the height at which the surface inversion ends. The algorithm of Nielsen-Gammon et al. (2008) determines the minimum virtual liquid water and ice potential temperature in the lowest 200 m of the atmosphere (θ_{vli_min}). Then, the boundary layer height is the height at which $\theta_{vli} = \theta_{vli\_min} + \Delta\theta_{vli}$, where $\Delta\theta_{vli}$ is set to be 0.5 K over water and
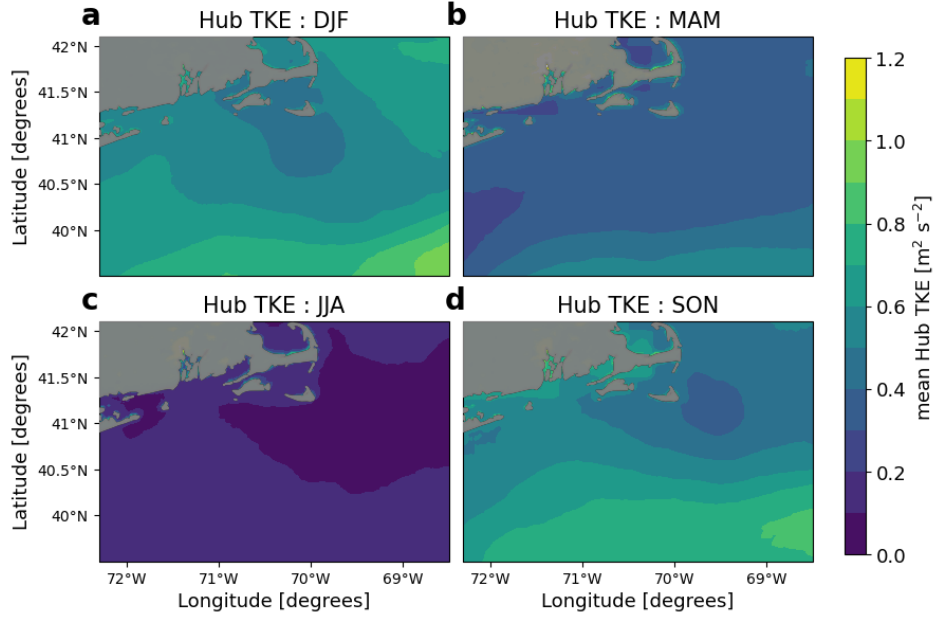
Figure 4. Same as in Fig. ~~5~~3, but for hub-height ~~QKE~~TKE.

1.25 K over land. In this region, the average PBLH varies spatially and seasonally (Fig. 5). Mean PBL heights range from 112 m to 1,086 m. During the summer, when stable conditions are more common, the shallowest PBL heights occur, with a mean PBL height of 453 m. Unstable conditions in the fall and winter lead to the deepest PBL heights, with mean values of 715 m in the fall and 698 m in the winter. PBL heights generally increase with distance from the coast. In the summer and fall, a minimum in PBLH is observed to the east of Nantucket.

2.2 Partitioning of the dataset

In this study, we quantify how hub-height wind speed, boundary-layer height, 2-m temperature, surface heat flux, and turbulence kinetic energy (~~QKE~~TKE) at the surface and hub height vary between the NWF and LA100 simulations.

While presenting our results, we highlight the variability of such changes as a function of atmospheric stability and wind speed at hub height (Table 2), both evaluated at the centroid of the MARIcent (Figure 1).

Wakes tend to be stronger and last longer in stably stratified conditions (Lundquist et al., 2019; Pryor et al., 2021; Rosencrans et al., 2024). ~~We classify atmospheric stability~~ To test that behavior here, we classify each time period with its surface-based atmospheric stability, determined by calculating the Obukhov length (L):

$$L = -\frac{u_*^3 \overline{\theta_v}}{\kappa g (\overline{w'\theta_v'})} \frac{u_*^3 \overline{\theta_v}}{\kappa g (\overline{w'\theta'})} \tag{1}$$
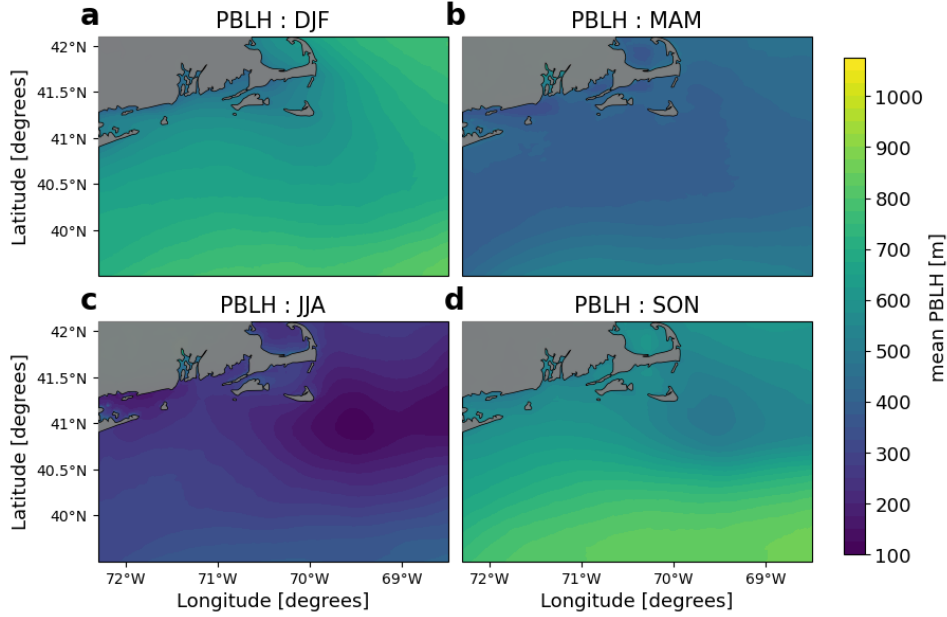
Figure 5. ~~Average PBLH~~ Same as in ~~the region is shown for each season from September 2019 – August 2020. (a) December~~Fig. 3, ~~January and February (DJF) (b) March, April, and May (MAM) (c) June, July, and August (JJA) (d) September, October, and November (SON)~~but for PBLH.

Table 2. The dataset is partitioned in six different ways, using labels in Column 1. The stability classification, wind speed range, wind direction range, and total number of hours in each partition are listed in Columns 2, 3, 4, and 5, respectively. In some Appendix figures, we consider different wind speed partitions for d, e, f,

Label	Stability	Wind speeds [m s^{-1}]	Wind directions [degrees]	Total # of hours
a	stable	all	all	3898
b	unstable	all	all	3899
c	neutral	all	all	987
d	stable	0-3 (Region 1)	180-270	61
e	stable	3-11 (Region 2)	180-270	1157
f	stable	11+ (Region 3)	180-270	1334

where u_* is the friction velocity, θ_v is the virtual potential temperature, κ is the von Kármán constant of 0.4, g is gravitational acceleration, and $\overline{w'\theta_v'}$ $\overline{w'\theta'}$ is the vertical turbulent surface heat flux. The virtual potential temperature is caluclated from the 2-m temperature, the surface pressure, and the surface water vapor mixing ratio. Values between 0 m and 500 m are considered

185
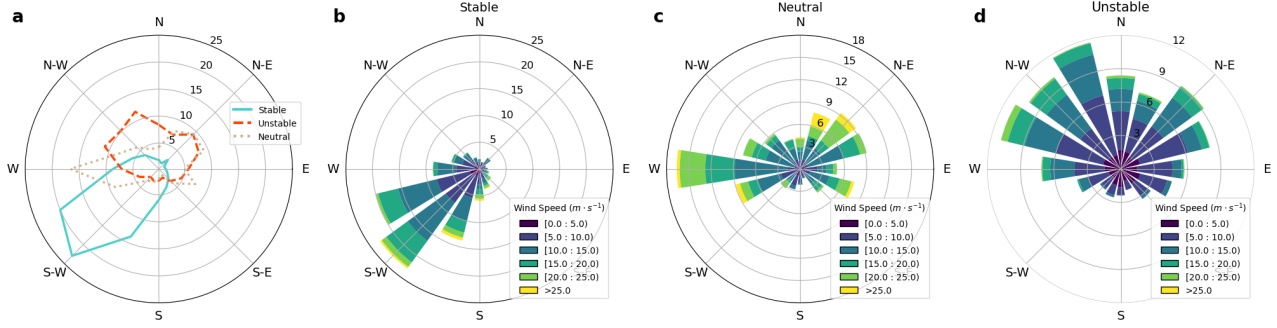
Figure 6. (a) The frequency of each 22.5-degree wind direction bin for each stability classification. Wind roses for stable, neutral, and unstable conditions are shown in Panels b, c, and d, respectively. In all panels, radial distance from the center refers to the percentage of values in each 22.5 degree bin.

stably stratified conditions, and values from -500 m to 0 m are considered unstable. Values outside of this range are considered neutral (Gryning et al., 2007; Sathe et al., 2011).

We note that the variability of atmospheric stability often reflects changes in wind direction in the region (Fig. 6). Winds in this region are often southwesterly and parallel to the coastline, but other wind directions do occur in the region (Fig. 1). Stable conditions almost always occur when winds are southwesterly. Wind directions vary more for unstable and neutral conditions: in unstable conditions, winds tend to be northerly, with a preference for northwesterly flow; in neutral conditions, winds are typically westerly or northeasterly. Because of this ~~tight coupling~~ correlation of stability and wind direction, further exploration of results as a function of wind direction is not presented, as they are redundant with the results as a function of atmospheric stability.

We also partition the dataset by considering three wind speed ranges based on the power curve of the turbines used in the NOW-WAKES simulation (Figure 2): 0-3 m s^{-1}, 3-11 m s^{-1}, and 11+ m s^{-1}. These modeled turbines do not produce any power when winds are 0-3 m s^{-1}. Then, power production steadily rises as wind speeds increase from 3-11 m s^{-1} (Region 2 on the power curve). At 11 m s^{-1}, turbine blades begin to pitch, resulting in ~~a leveling of the~~ the rated power production of the turbine being reached and not increasing further (Region 3). ~~To isolate~~ In the Appendix, we also consider cases with wind speeds in excess of 15 m s^{-1} when the turbine thrust coefficient becomes very small. To more clearly identify the effect of the variability in hub-height wind speed on wake impacts from those caused by differences in stability and wind direction, when showing the variability of the wake impacts with hub-height wind speed, we only consider periods with stable conditions and southwesterly (180 - 270 °) winds.

3 Characterizing wind plant wake area and length with machine learning

We characterize the wind plant wake area and wake length for each of the 3,898 hours of the year with a stably stratified atmosphere.

We first determine the difference in wind speed between the LA100 and NWF simulations. The wind speed U is calculated at the model level closest to the turbine hub height (~ 138 m). Waked locations are identified as points with a wind speed deficit of at least 1 m s^{-1}. This wake definition is stronger than the 0.5 m s^{-1} threshold used in Golbazi et al. (2022); Rybchuk et al. (2022); Rosencra, and was chosen to aid in identifying contiguous wakes. A relative wake definition proved problematic by making the wake field even noisier.

Next, the points that show a wind speed deficit that should be attributed to the wind plant wake need to be identified. As an example, in Fig. 7a, the wind plant wake should be contained in the cluster of points around the wind plants, but some other remote locations, not contiguous with the wind plant wake, also show a wind speed deficit of at least 1 m s^{-1}. The deficits at these remote locations are presumed to be numerical noise as identified in Ancell et al. (2018); Lauridsen and Ancell (2018) and discussed in Appendix F of Rosencrans et al. (2024). To handle these situations, we employ the Density-Based Spatial Clustering of Applications with Noise (DBSCAN) method (Ester et al., 1996) to accurately identify the wind plant wake. The algorithm groups points together based on their distance to dense regions. DBSCAN requires two main parameters. The first is the maximum distance between two points for one to be considered in the neighborhood of another. The second parameter is the minimum number of points in a neighborhood for a point to be considered as a core point. Here, we use a maximum distance value of 0.1 degrees and a minimum points value of 30. Using these parameters, points are grouped into clusters that are assigned a label, as in Figure 7b and 7e.

The next step is to select the cluster that is likely to be the wind plant wake. For each cluster identified by the DBSCAN algorithm, we determine the percentage of points in the cluster that are within the wind plant. All clusters with fewer than 15% of points in the wind plant are excluded from consideration. Then, the cluster with the most points overall is selected.

Once the wind plant wake cluster is selected, we create a concave hull shape around its points (Fig. 7c and 7f). We define the area of the wind plant wake as the area of this concave hull polygon. The wake length is the maximum distance from MARIcent to any bounding point of the identified wind plant wake polygon (red outline in Fig. 7c and 7e).

Many cases have a clearly defined wake and a straightforward wake detection process, as shown in Fig. 7d, 7e and 7f). However, 15.2% of hours have ill-defined wakes, so that they are flagged by our algorithm and not included in the final results of our analysis. An hour can be flagged if either of the following two situations occurs:

1. Less than 40% of the coordinates located in the wind plant are classified as part of the wind plant wake. This ensures that the identified wind speed deficit is connected to the wind plant, which is the source of the wake.

2. The ratio of the number of points in the wind plant wake cluster to the total number of points with a wind speed deficit of at least 1 m s^{-1} is less than 0.2. This flags exceptionally noisy times when the selected wake represents a small number of the locations with a significant wind speed deficit.

In addition, no wake is identified at all if there are less than 4 points with a wind speed deficit greater than 1 m s^{-1}, or if less than 5% of points identified by DBSCAN are located within the wind plant. An additional 5.5% of hours are excluded from our analysis due to these criterion.
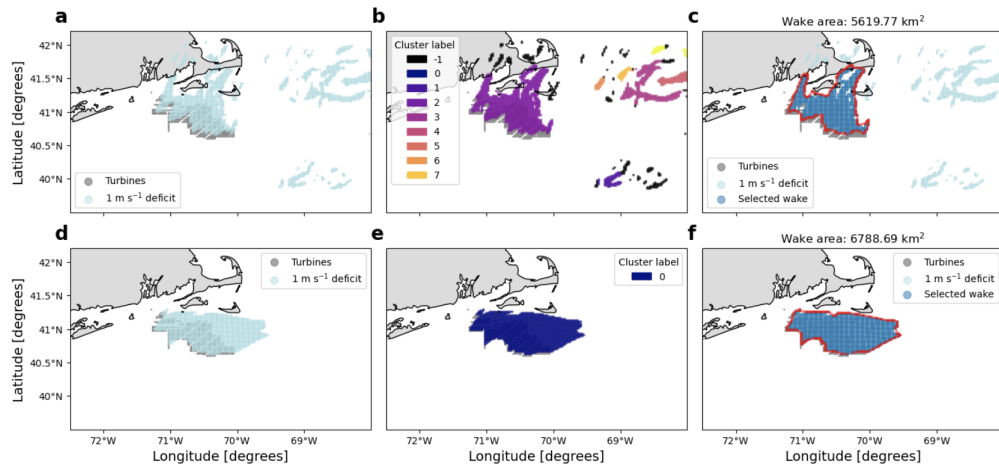
Figure 7. Example of the three steps taken to identify the wind plant wake on 14 December 2019 at 22:00 UTC (a, b, and c) and on 04 February 2020 at 07:00 UTC (d, e, and f). Turbines are marked in gray. (a and d) All points identified with a 1 m s^{-1} deficit are marked in light blue. (b and e) The points with a wind speed deficit are clustered, and a label is assigned to each cluster by the DBSCAN algorithm. The -1 label indicates points classified as noise. (c and f) The selected wind plant wake is in darker blue, with its wake boundary in red.
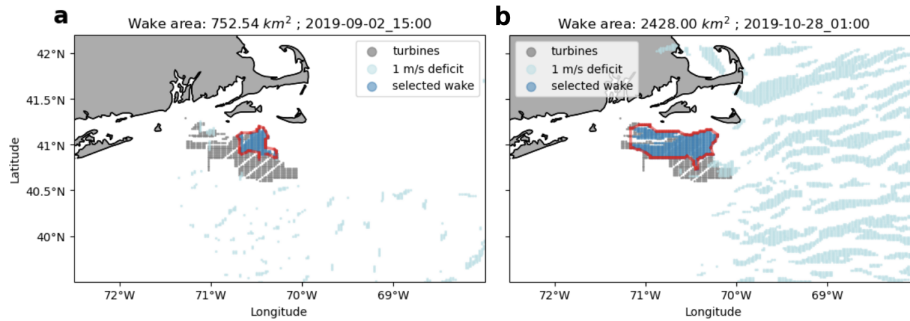
Figure 8. Example of two cases that are flagged by the wake detection algorithm and therefore not considered for further analysis. These plots follow the same convention as the right panel in Fig. 7.

240 ~~The cases~~ We demonstrate this flagging process in Figure 7~~would not be flagged. .~~ While the case in the top row of Figure 7 has some noise, the identified wake clearly originates from the wind plant and covers most of the wind plant area. In addition, the points not selected for the wake represent a small fraction of all points with a wind speed deficit greater than 1 m s^{-1}. On the other hand, Figure 8 shows two examples of cases that are flagged by our algorithm: in (a), fewer than 40% of the wind plant is covered by the wake; in (b), the identified wake includes less than 20% of all the locations with a wind speed deficit

245 greater than the 1 m s^{-1} threshold.
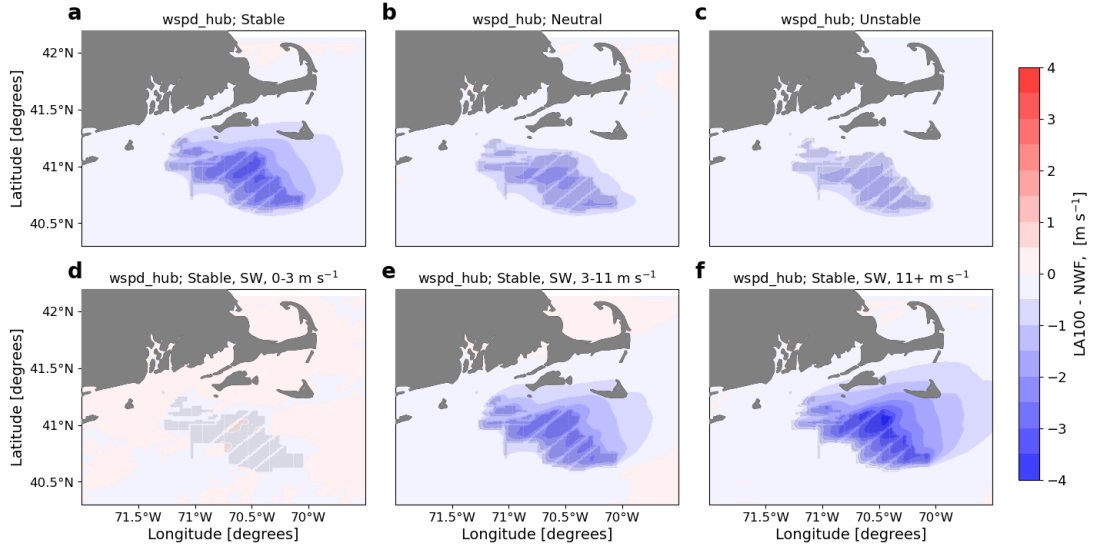
Figure 9. Mean hub-height wind speed difference between the LA100 and NWF simulations in (a) stable conditions, (b) neutral conditions, (c) unstable conditions, (d) 0-3 m s^{-1}, (e) 3-11 m s^{-1}, and (f) 11+ m s^{-1}. Panels d, e, and f are only during times with stable conditions and southwest winds. Turbines are marked in gray.

4 Results

4.1 Wind plant wake impacts on wind speed

4.1.1 Hub-height wind speed

Hub-height wind speeds in wakes are reduced most in stable conditions and least in unstable conditions (Fig. 9a and 9c). Within the wind plant, average wind speeds are reduced by up to 2.7 m s^{-1} in stable conditions, and up 1.5 m s^{-1} in unstable conditions, as turbines extract momentum from the flow. In stable conditions, there is also a significant decrease in wind speed downwind of the wind plant (to the northeast, given the dominant southwesterly wind direction during stable condition; see Fig. 6), while in neutral and unstable conditions the extent of the wake is much smaller. During unstable conditions, wind speeds are replenished faster due to increased mixing from aloft (Abkar and Porté-Agel, 2013), which reduces the extent of the wake. These results confirm the results , as also reported in Figure 12 of Rosencrans et al. (2024).

In stable conditions and when the wind is from the southwest, hub-height wind speeds are reduced more with increasing ambient wind speeds (Fig. 9d, 9e, and 9f) up to about 15 m s^{-1}. There is almost no difference between the simulations with and without turbines for quiescent winds, when wind turbines are not operational, as expected, as the only turbine influence is that of the standing thrust coefficient. Hub-height wind speeds are reduced by up to 2.5 m s^{-1} for wind speeds in Region 2 of the turbine power curve, and up to 3.6 m s^{-1} for wind speeds above 11 m s^{-1} in Region 3 of the power curve. The wake also extends further for faster wind speeds: a wind speed deficit of at least 0.5 m s^{-1} extends out to the northern edge of Nantucket

Island for moderate wind speeds, and several kilometers further than this for faster wind speeds. Of note, when the wind speeds exceed 15 m s^{-1} when the thrust coefficient is very small, the wind speed deficit starts to decrease again (see Appendix Fig. B1).

265 Hub-height wind speeds decrease within and downwind of the wind plant, with the largest impacts occurring during stable conditions and for faster ambient wind speeds at the slower end of Region 3 (11 -15 m s^{-1}). Wind speed deficits in the wake of wind plants are well documented for cases both onshore and offshore (Christiansen and Hasager, 2005; Fitch et al., 2013; Dörenkämper et al., 2015; Platis et al., 2018; Fischereit et al., 2022a). Our results on the impact of atmospheric stability on wakes confirm the results of Rosencrans et al. (2024), who uses the same dataset. In the central United States, Fitch et al.

270 (2013); Rajewski et al. (2013); Smith et al. (2013) also find that the largest wind speed deficits occur for faster wind speeds, stable conditions, and when turbulent mixing is inhibited.

For individual turbines, the magnitude of the wake also varies with wind speed differently than observed here. For individual turbines (Rhodes and Lundquist, 2013), (Rhodes and Lundquist, 2013): maximum wake wind speed deficits occur near rated power when the turbine thrust coefficient is near its maximum value, with decreasing wake wind speed deficits as wind speeds

275 increase and thrust coefficient decreases. Here, the wake wind speed deficits continue to amplify as wind speeds increase.

4.1.2 Wind plant wake impacts on 10 m wind speed

Wind plant wake impacts on 10 m wind speed depends on the stability of the atmosphere (Fig. 10a, 10b, and 10c). In stable conditions, average 10 m wind speeds increase by up to 0.32 m s^{-1} within the wind plant, while in neutral and unstable conditions, wind speeds decrease by up to 0.45 and 0.82 m s^{-1}, respectively. The acceleration near the surface within the wind

280 plant in stable conditions can be understood as acceleration around an obstacle in stably-stratified flow: when the flow cannot pass through the rotor disk and cannot rise above the rotor disk due to stable stratification, it must pass through a more confined region (under the rotor disk) and therefore accelerates to conserve mass. In neutral or unstable conditions, vertical motion is not constrained and so the flow does not need to accelerate under the rotor disk. Outside of the wind plant, 10 m wind speeds are reduced in all stability classifications, with the largest deficit in stable conditions, as also observed for hub-height wind

285 speed. The spatial extent of the wake is smaller for unstable conditions than for neutral and stable conditions. During : during unstable conditions, wind speeds are replenished faster due to increased mixing from turbines above, which reduces the extent of the wake.

Under stable conditions and southwesterly winds, the downwind deficit in 10 m wind speeds are reduced generally increases more with increasing ambient wind speeds (Fig. 10d, 10e, and 10f). There are minimal differences between the simulations

290 for quiescent winds, when wind turbines are not operational, as expected. Downwind of the wind plant, 10 m wind speeds are reduced by up to 0.60 m s^{-1} for wind speeds in Region 2 of the turbine power curve, and up to 0.70 m s^{-1} for wind speeds above 11 m s^{-1}. As already noted for hub-height wind speed, when the wind speeds exceed 15 m s^{-1} and the thrust coefficient gets very small, the wind speed deficit begins to decrease again (see Appendix Fig. B2). The wake also extends further for faster wind speeds: a wind speed deficit of at least 0.1 m s^{-1} extends out to the northern edge of Nantucket Island for moderate

295 wind speeds, and several kilometers further than this for faster wind speeds. For moderate and fast wind speeds, there is also a
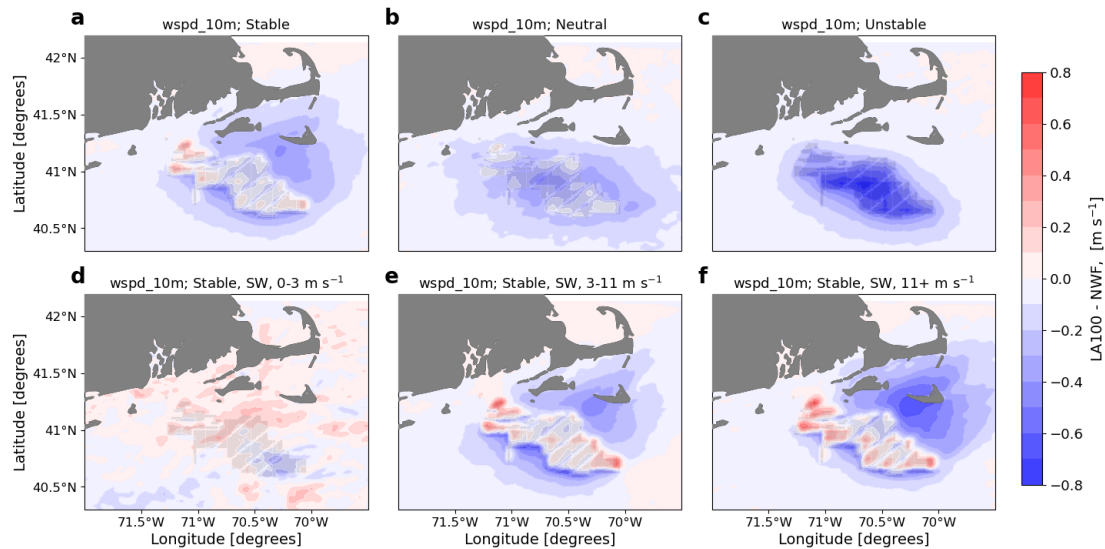
Figure 10. Mean 10 m wind speed difference between the LA100 and NWF simulations in (a) stable conditions, (b) neutral conditions, (c) unstable conditions, (d) 0-3 m s^{-1}, (e) 3-11 m s^{-1}, and (f) 11+ m s^{-1}. Panels d, e, and f are only during times with stable conditions and southwest winds. Turbines are marked in gray.

reduction in wind speeds upwind of the wind plant. The extent of this effect is slightly larger for moderate wind speeds than for stronger wind speeds. Within the wind plant, surface accelerations also differ slightly between moderate and fast wind speeds: wind speeds increase by up to 0.50 m s^{-1} for moderate ambient wind speeds and by up to ~~0.57~~ 0.8 m s^{-1} for ~~fast wind speeds~~ ~~.~~ wind speeds faster than 11 m s^{-1}. For wind speeds faster than 15 m s^{-1}, the accelerations are more widespread within the

300   wind plant, but the maximum accelerations are not faster than those in the range of 11 - 15 m s^{-1} (see Fig. B2).

~~Changes in wind speed~~ Downwind wake wind speed deficits at 10 m are much smaller than at hub-height: wind speed reductions in the wake at the surface are about 4.5 times weaker than at hub-height. At 10 m, wind speeds accelerate slightly (less than 1 m s^{-1}) within the wind plant during stable conditions only, a phenomenon that was also observed in the simulations and lidar observations of Bodini et al. (2021) and the large-eddy simulations of Vanderwende et al. (2016). Upwind of the wind

305   plant, wind speeds are reduced slightly, especially when winds are in Region 2 of the power curve and the thrust coefficient is near its maximum value. Wu and Porté-Agel (2017) identifies this effect in large-eddy simulations of neutral boundary layers.

4.2   Wind plant wake impacts on 2-m temperature

Differences in 2-m temperature are small, less than 0.3 K, when wind plants are present. Any differences are the most significant during stable conditions (Figure 11a). During stable conditions, temperatures increase by around 0.1 degrees Celsius within

310   the wind plant and decrease by a similar amount downwind of the wind plant. In neutral conditions, temperatures increase by only around 0.05 degrees both within and around the wind plants (Figure 11b). In unstable conditions, temperature differences are very small, but a slight decrease in temperature is observed within the wind plant (Figure 11c). During stable conditions,
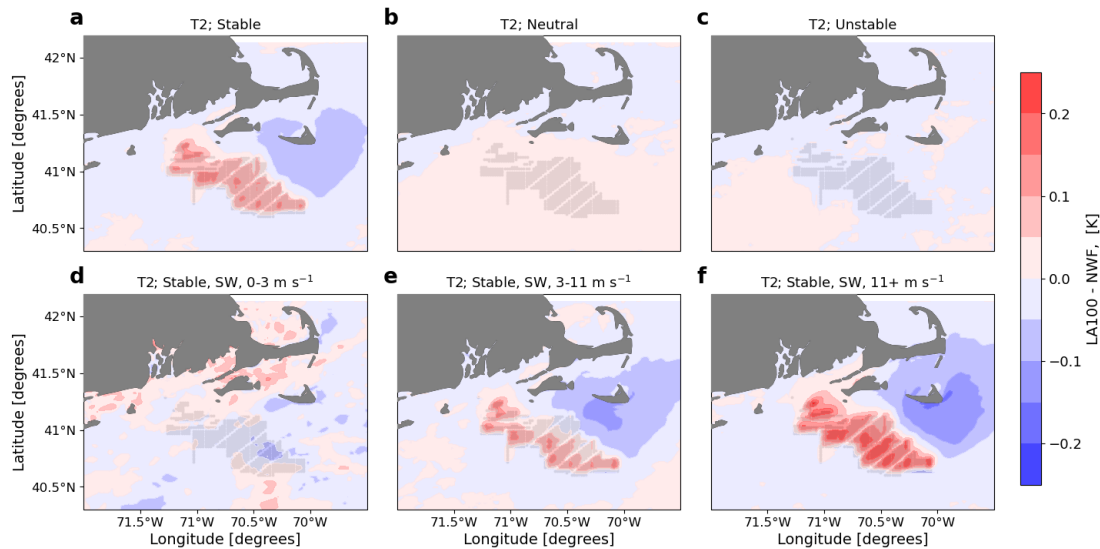
Figure 11. Mean 2 m temperature difference between the LA100 and NWF simulations in (a) stable conditions, (b) neutral conditions, (c) unstable conditions, (d) 0-3 m s^{-1}, (e) 3-11 m s^{-1}, and (f) 11+ m s^{-1}. Panels d, e, and f are only during times with stable conditions and southwest winds. Turbines are marked in gray.

turbines mix warmer air from aloft down to the surface, resulting in ~~what appears to be~~ a temperature increase but is really just redistribution of heat (as also discussed in Fitch et al. (2013) and Siedersleben et al. (2018a), among others). In unstable conditions, the boundary layer is already well mixed, ~~which likely dominates any temperature changes caused~~ so that any mixing by wind turbines is simply remixing a well-mixed layer.

In stable conditions for southwesterly winds, changes in 2-m temperature become more significant with increasing hub-height wind speed (Figure 11d, 11e, and 11f). Temperature differences at the surface are negligible for quiescent winds when turbines are not operational. Temperature increases by up to 0.14 K for moderate wind speeds, and up to 0.2 K for wind speeds greater than 11 m s^{-1}. The largest temperature increases occur near the front of the wind plant, which is the southwestern side of the lease area here. During moderate wind speeds, there is no difference between the NWF and LA100 simulations on the northeastern side of the lease area. Temperatures are reduced downwind of the wind plant for moderate and fast wind speeds; however, the strongest reduction occurs for fast wind speeds. The extent of this moderate temperature reduction is large, extending to Massachusetts.

Differences in 2-m temperature are small, but we find increased temperatures within the wind plant and decreased temperatures downwind. The strongest temperature differences occur during stably stratified conditions and hub-height wind speeds faster than 11 m s^{-1}). Few differences occur between the NWF and LA100 simulation when conditions are unstable or during quiescent winds. Several other studies have identified warming below the turbine hub, with the strongest impacts occurring during stable conditions Baidya Roy and Traiteur (2010); Lu and Porté-Agel (2011); Fitch et al. (2013); Siedersleben et al. (2018a); Golbazi et al. (2022). The simulations used here use wind turbines with a hub-height of 138 m, which resembles the

"extreme-scale" turbine of Golbazi et al. (2022). While they find cooling at the surface for extreme-scale turbines, we still find warming at the surface during stable conditions.

The amount of added TKE may also have an impact on observed temperature changes. Baidya Roy and Traiteur (2010) found larger differences in temperature for small amounts of ambient TKE than for large amounts of TKE. Our simulations use the 100% added TKE option, which promotes more mixing and could explain the small differences observed here. We also observe slightly smaller temperature changes than in Fitch et al. (2013), which identified warming below the rotor of up to 0.8K.

For stably stratified mesoscale simulations onshore (Texas), Xia et al. (2019) find that the turbine-added turbulence drives the surface warming signal by enhancing vertical mixing. In contrast, the turbine drag component causes the remote downwind surface cooling by reducing shear and promoting near-surface thermal stratification. A similar process occurs here, most visible in the stably stratified conditions (Fig. 11a).

4.3 Wind plant wake impacts on surface sensible heat flux

Within the wind plant, surface sensible heat fluxes are reduced for all stability classifications (Fig. 12a, 12b, and 12c). Heat fluxes are least affected during neutral conditions, with a reduction less than 1 W m^{-2} throughout the region. The heat flux reduction within the wind plant is largest during unstable conditions, with differences up to around 3 W m^{-2}. Heat fluxes are typically positive during unstable conditions, so a reduction in heat flux corresponds to less heat being transferred upwards, which is consistent with the (slight) reduction in 2-m temperature during unstable conditions. During stable conditions, heat flux is negative. When heat flux is moderately reduced within the wind plant, it becomes more negative implying that more heat is transferred to the surface, which is consistent with the T2 changes of Figure 11. We also observe an increase in heat flux downwind of the wind plant of around 1.5 W m^{-2} during stable conditions, implying that less heat is transferred to the surface the cooling typical of stable conditions accelerates. No downwind effect on heat flux occurs during neutral and unstable conditions.

Impacts of the wind plant on heat flux increases with increasing wind speeds (Fig. 12d, 12e, and 12f), during stable conditions and for southwesterly winds. Weak winds correspond to negligible differences in heat flux due to nonoperational turbines. Heat flux decreases within the wind plant for moderate and fast wind speeds, with largest changes for wind speeds in Region 3 of the power curve. Similar to the results seen for 2-m temperature, the strongest changes in heat flux occur near the front of the wind plant, on the southwestern side. Downwind of the wind plant, heat flux increases by up to 1.5 W m^{-2} for moderate wind speeds, and up to 2.75 W m^{-2} for fast wind speeds. The spatial extent of this downwind effect is similar to that observed for 2-m temperatures, as changes in surface heat flux are related to changes in surface temperature. We find that the heat flux is weakened where cooling is found (northeast of the wind plant for stable conditions, southwest winds, and strong winds), which is in agreement with findings in Golbazi et al. (2022).

The surface heat flux decreases within the wind plant. The strongest reduction in heat flux occurs during unstable conditions and fast wind speeds. Golbazi et al. (2022) suggests that cooling is associated with a weakening of the heat flux. Our findings support this observation: during stable conditions, we observe cooling and an increase in surface heat flux to the northeast of
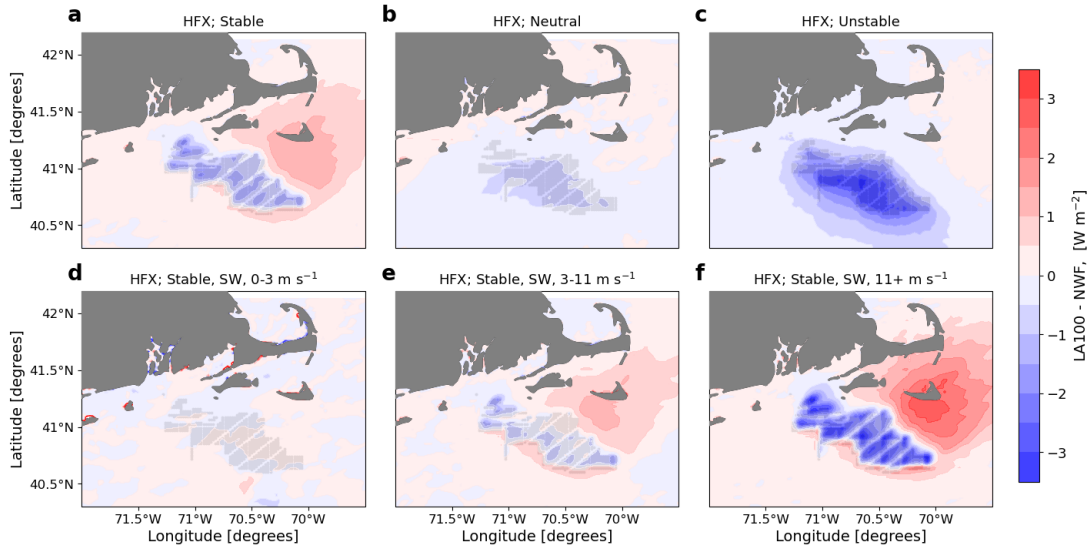
Figure 12. Mean heat flux difference between the LA100 and NWF simulations in (a) stable conditions, (b) neutral conditions, (c) unstable conditions, (d) 0-3 m s^{-1}, (e) 3-11 m s^{-1}, and (f) 11+ m s^{-1}. Panels d, e, and f are only during times with stable conditions and southwest winds. Turbines are marked in gray.

365   the wind plant; in the wake of the wind plant in stable and neutral conditions, we find an increase in the surface heat flux, which is consistent with Rajewski et al. (2014). Xia et al. (2019) also suggests that temperature changes within the wind plant are driven by changes in heat flux, with a decrease in sensible heat flux near turbines and an increase downwind, which aligns with our stable stratification results in Fig. 12a.

4.4   Wind plant wake impacts on ~~QKE~~ TKE

370   Wind turbines impact ~~QKE~~ TKE at both hub height and at the surface. The wind turbine parameterization injects turbulence into the simulations at the altitudes of the turbine rotor disks, with more turbulence injected into cells with more turbines.

4.4.1   Hub-height ~~QKE~~ TKE

In the vicinity of the wind plants, ~~QKE~~ TKE increases at hub height. A similar magnitude in this increase occurs for all stability classes, suggesting that stability does not immediately modify the ~~QKE~~ TKE generated by turbines (Fig. 13a, 13b, and 13c).
375   The largest increases in ~~QKE~~ TKE occur in the grid cells populated by turbines, where the turbulence is ~~introduced~~ directly introduced by the WRF wind farm parameterization. This hub-height ~~QKE~~ TKE increase rapidly erodes downwind of the wind plants. The amount of added turbulence directly relates to the number of turbines in each grid cell, resulting in a grid pattern of larger ~~QKE~~ TKE values corresponding to cells with more turbines.
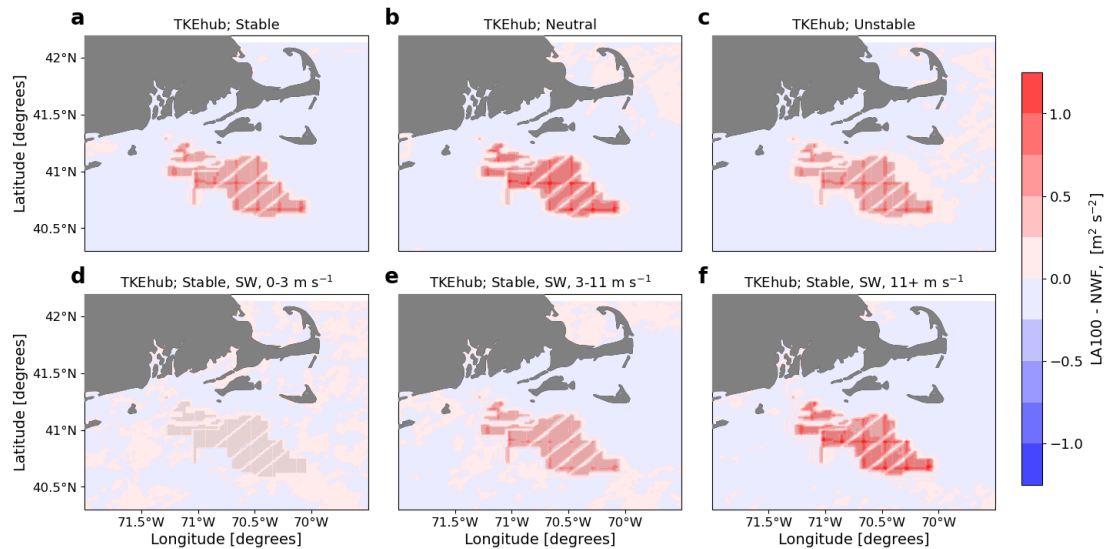
Figure 13. Mean hub-height ~~QKE~~ TKE difference between the LA100 and NWF simulations in (a) stable conditions, (b) neutral conditions, (c) unstable conditions, (d) 0-3 m s^{-1}, (e) 3-11 m s^{-1}, and (f) 11+ m s^{-1}. Panels d, e, and f are only during times with stable conditions and southwest winds. Turbines are marked in gray.

When focusing on stable conditions with southwesterly winds, the magnitude of the increase in hub-height ~~QKE~~ TKE within the wind plant increases with increasing ambient wind speed (Fig. 13d, 13e, and 13f). Negligible ~~QKE~~ TKE is generated for quiescent winds, when turbines are not operational and the parameterization does not add any turbulence. The most added turbulence at hub height is evident in the fastest wind case (Fig. 13c). The fastest wind speeds may also result in more mixing on their own. Increases in ~~QKE~~ TKE are localized to the cells with turbines, with the strongest values occurring where turbine density is the greatest.

4.4.2 Surface ~~QKE~~TKE

Differences in surface ~~QKE~~ TKE are subtler than differences at hub height but show more variability with stability (Fig. 14a, 14b, and 14c). During stable conditions, ~~QKE~~ TKE at the surface is largely unaffected by the presence of wind turbines. Vertical mixing is suppressed during stable conditions, making it unlikely that turbulence from the turbines, injected at the rotor disk altitudes, can reach the surface. Surface ~~QKE~~ TKE increases within the wind plant during neutral conditions, although changes are limited to areas close to turbines. During unstable conditions, ~~QKE~~ TKE increases throughout the entire lease area, albeit by a factor of four less than at hub height. ~~Surface QKE~~, thanks to enhanced vertical mixing that causes the TKE injected at hub height to also reach the surface. Surface TKE slightly decreases in areas outside of the wind plant for all stability classifications, although the largest reductions occur during neutral and unstable conditions.

Ambient hub-height wind speed also influences the change in ~~QKE~~ TKE at the surface (Fig. 14d, 14e, and 14f) in stable conditions and for southwesterly winds. As we found at hub height, quiescent winds are not associated with any noticeable
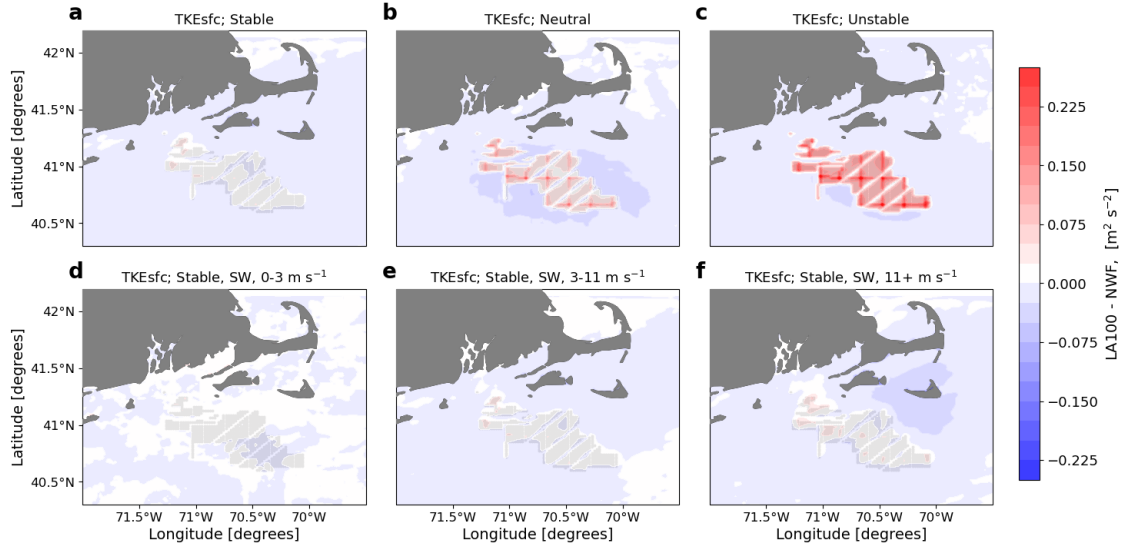
Figure 14. Mean surface ~~QKE~~ TKE difference between the LA100 and NWF simulations in (a) stable conditions, (b) neutral conditions, (c) unstable conditions, (d) 0-3 m s^{-1}, (e) 3-11 m s^{-1}, and (f) 11+ m s^{-1}. Panels d, e, and f are only during times with stable conditions and southwest winds. Turbines are marked in gray.

change in surface ~~QKE~~TKE, due to turbines being nonoperational. Moderate wind speeds also have very small differences, but there is a slight increase in surface ~~QKE~~ TKE on the upwind side of the lease area. During strong wind speeds, differences between the LA100 and NWF simulations are most apparent. Surface ~~QKE~~ TKE increases on the upwind side of the lease area and decreases downwind. Downwind of the wind plant, wind speeds are reduced in the wake, which results in less ~~QKE~~ TKE producing wind shear.

~~QKE~~ TKE increases within the wind lease area both at hub height, where the turbulence is injected, and at the surface. Not surprisingly, impacts at the surface are much smaller than at hub height, where the increase in ~~QKE~~ TKE is about 10 times greater than at the surface. At hub height, differences between both simulations diminish quickly with distance from the wind plant, as we observe minimal changes outside of the lease area. This simulated behavior concurs with the simulations in Bodini et al. (2021). Atmospheric stability does not seem to impact the magnitude of ~~QKE~~ TKE increase at hub height (as the amount of added TKE is not a function of stability but rather of wind speed and the number of turbines), but it does at the surface. Differences in ~~QKE~~ TKE increases with increasing wind speed at both levels.

4.5 Wind plant wake impacts on boundary layer height

In the vicinity of wind plants, the PBL height increases for all stability classifications (Figure 15a, 15b, and 15c). The atmospheric stability modulates the strength of this effect. The PBL height increases by up to 99 m during stable conditions from a mean value of 268 m, and up to 67 m and 39 m for neutral and unstable conditions, respectively, from means of 556 and 644 m, respectively. During stable conditions, PBL heights are generally lower and often within the rotor region, which results in a
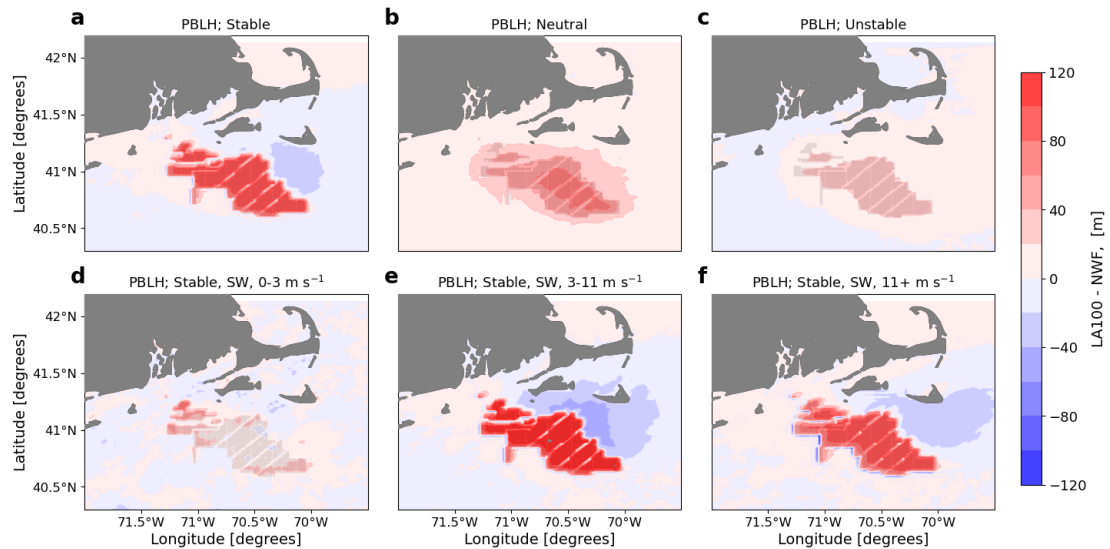
Figure 15. Mean PBLH difference between the LA100 and NWF simulations in (a) stable conditions, (b) neutral conditions, (c) unstable conditions, (d) 0-3 m s^{-1}, (e) 3-11 m s^{-1}, and (f) 11+ m s^{-1}. Panels d, e, and f are only during times with stable conditions and southwest winds. Turbines are marked in gray.

larger overall change in PBL height. During neutral and unstable conditions, PBL heights are generally deeper; thus, turbines are less likely to interact with air in the free atmosphere.

Downwind of the wind plant, PBL heights also change. Distant from the wind plant, PBL heights are reduced by up to 45 m during stable conditions as compared to the no-wind-farm, likely due to the decreased shear in the wake of the wind plant. During neutral and unstable conditions, PBL heights increase throughout the region during neutral conditions, while the impact of wind plants is limited to the lease areas during unstable conditions.

In stable conditions and for southwesterly winds, in the vicinity of wind plants, the PBL height is raised for all wind speeds, but this effect is strongest for wind speeds of 3-11 m s^{-1}, and negligible for quiescent winds (Figure 15d, 15e, and 15f). Wind turbines are not operational when wind speeds are below 3 m s^{-1}, and thus we do not expect wind plants to have a large effect on PBL height. The magnitude of the increase in PBLH within the wind plant is larger for hub-height wind speeds of 3-11 m s^{-1} than for wind speeds of 11+ m s^{-1}. Turbines have a smaller effect on winds once they reach Region 3 on the power curve, which likely explains this difference. Both moderate and fast wind speeds show a reduction in PBL height downwind of the wind plant, with the largest reduction associated with wind speeds in Region 2 of the power curve.

The PBLH increases within the wind plant and generally decreases downwind of the wind plant as compared to simulations with no wind plants. The largest differences occur during stable conditions and when winds are in Region 2 of the turbine power curve. This variability concurs with the large-eddy simulations of Wu and Porté-Agel (2017), which found increased PBL heights in the wind plant and depressed PBL heights in the exit region of the wind plant. Fitch et al. (2013) also finds, in
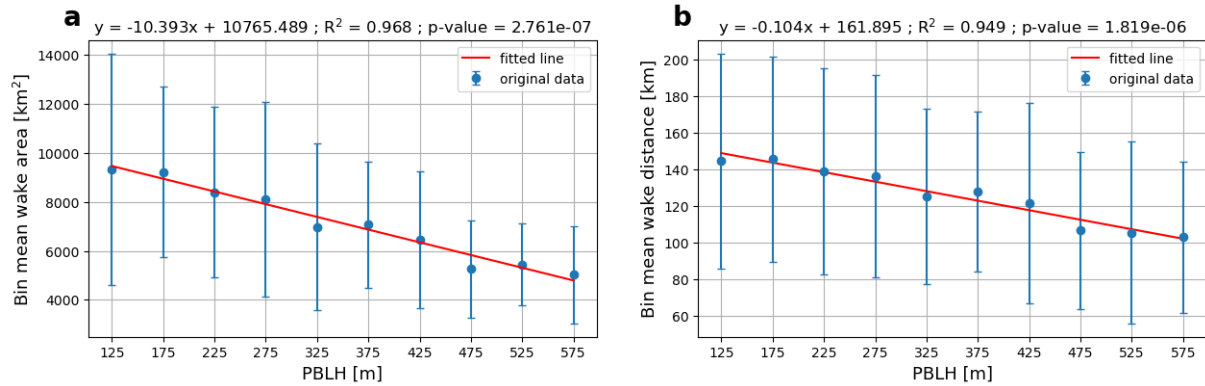
Figure 16. The mean (a) wake area and (b) length as a function of the mean lease area PBLH during stable conditions, where the PBLH values are binned every 50 m from 125 m to 575 m. The mean PBLH values are calculated as the average PBLH across the wind lease area. For each bin, the blue dots show the mean value, and the blue vertical lines represent the ± 1 standard deviation error bar. The best-fit line for the bin means is in red. Each panel displays the line of best fit equation, R^2 value, and p-value on the top.

430   mesoscale simulations, that wind plants elevate the height of the PBL height by up to 145 m. PBLH values were also slightly depressed downwind of the wind plant during stably stratified conditions.

4.6   Relationship between PBLH and wake extent

The wind plant wake extent in stable conditions depends on the PBLH in the Massachusetts-Rhode Island lease area in a statistically significant way (Fig. 16). Wake area and length are determined using the methodology described in Section 3.

435   Wake area and length generally decrease with increasing PBLH for PBLH values between 100 m and 600 m. As PBLH increases, the volume of air available to recover the wake increases, so wakes in deeper PBLs tend to have a smaller area and length. When the PBLH is shallow, lower than 100 m, the wind plant wake area increases with increasing PBLH (not shown). These lower PBLH values are below hub height and are associated with smaller wakes because the wake mostly propagates in the free atmosphere, where a large volume of air is available to quickly recover the wake. In Figure 16, a linear relationship

440   appears between mean lease area PBLH and the mean wake area or length for each bin. For every 1 meter increase in PBLH, the wake area decreases by approximately 10.4 km^2, and the wake distance decreases by about 0.1 km. The significance of these results is supported by the p-values, which are significantly below the 0.05 threshold. Still, the standard deviation is quite large, indicating considerable variability, likely associated to the fact that other factors such as ambient TKE and wind speed may also influence the wake extent in conjunction with the PBLH.

445   The analysis of stable wake areas and lengths demonstrates that deeper PBLs support faster wake recovery in a statistically significant way. The PBLH is inversely proportional to wake area and length, but other variables likely contribute to influencing the variability of wake extent. In a 55-day set of mesoscale simulations, Pryor et al. (2021) also suggest a negative relationship

between PBLH and a normalized wake extent parameter. The large-eddy simulations of Maas and Raasch (2022) also find that wakes, at least for very large wind farms, tend to be longer with shallower boundary layers.

5 Conclusions

Here, we assess the meteorological impact of offshore wind farms over an annual cycle using one year of WRF simulations with and without wind plants incorporated into the model. We assess the difference in hub-height wind speed, 10 m wind speed, 2 m temperature, surface heat flux, hub-height turbulence, surface turbulence, and boundary-layer height during different stability classifications and ambient wind speeds in the Massachusetts-Rhode Island lease area. We also ~~demonstrate~~ develop and demonstrate a machine-learning approach to identify wind plant wakes, and use this method to demonstrate the relationship between ~~boundary layer height and~~ boundary-layer height and both the area and length of the wind plant wake.

Hub-height wind speeds are reduced within and downwind of the lease area, especially during stable conditions and wind speeds above 11 m s^{-1}. A subtle (less than 0.2 K) increase in 2-m temperature within the wind plant can occur; this increase is strongest during stable conditions and faster wind speeds. Also during stable conditions, temperature decreases slightly downwind of the wind plant, as has been observed in mesoscale simulations in other regions. Changes in heat fluxes are also small. Heat flux is reduced within the wind plant and increased downwind. The largest reduction occurs during unstable conditions, while the largest downwind increase occurs for stable conditions and faster wind speeds. We find that turbulence ~~, as simulated by QKE,~~ increases at hub height in the immediate vicinity of turbines. Only in unstable conditions does this increase in ~~QKE~~ TKE manifest at the surface as well. Wind turbines nudge the boundary layer up in the immediate vicinity of the wind turbines, especially during stable conditions and when winds are in Region 2 of the power curve. During stable conditions, the boundary-layer height is slightly reduced downwind. Finally, we find that shallower boundary-layer heights promote larger wakes.

These simulations use one type of turbine and the planned 1 ~~nm~~ nautical mile spacing for these wind farms. Further investigations could assess how these impacts change with varying turbine layouts and sizes, as in Golbazi et al. (2022); Pryor et al. (2021). While Golbazi et al. (2022) considers larger turbines similar to turbines used here, more research into their impacts on local meteorology is needed.

Our analysis is based on one complete year of simulations, rather than one season (Golbazi et al., 2022) or selected multiday studies (Pryor et al., 2021). However, interannual variability does affect wind resources (Lee and Lundquist, 2017; Bodini et al., 2016) and so may affect the effects of wakes as well. Therefore, a multiyear study could provide more insights into interannual variability.

Further, simulated winds (Draxl et al., 2014; Bodini et al., 2024a; Liu et al., 2024) and simulated wakes (Rybchuk et al., 2022) show dependence on the PBL scheme chosen for the model simulations. At the moment, the Fitch wind farm parameterization is coupled only with the MYNN PBL scheme used here and with the 3DPBL scheme (Kosović et al., 2020; Juliano et al., 2021). Future work could assess how micrometeorological responses to wind farm wakes depend on the choice of PBL scheme.

480   Of course, this study relies on the accurate representation of wakes in the Fitch WRF wind farm parameterization. While wakes simulated with this parameterization compare reasonably well with the limited sets of observations available (Lee and Lundquist, 201 , the availability of observations of wake effects at multiple distances and heights from wind farms, especially offshore, is limited. Ongoing experiments such as AWAKEN (Moriarty et al., 2024) may provide more extensive datasets to support modifications to wind farm parameterizations in mesoscale models. Additionally, comparisons of these mesoscale representations

485   to more finely resolved large-eddy simulations of wind farms (Vanderwende et al., 2016; Peña et al., 2022) may suggest other improvements, although these comparisons should be carried out for a range of atmospheric stability conditions and wind farm geometries. Particular attention should be paid to effects on surface meteorology as well as dynamics directly relevant to wind turbine power production.

Further, because these present simulations are not coupled with a wave model and ocean model, other feedbacks between the

490   ocean and atmosphere may be relevant. Over water, wind plant wakes may influence ocean dynamics ~~(Raghukumar et al., 2022, 2023)~~ (Raghukumar et al., 2022, 2023; Liu et al., 2023), including upwelling. Therefore, coupling with wave and ocean models could provide insight into potential wake impacts on the ocean. Daewel et al. (2022) considers the impact of offshore wakes on primary production, but additional analysis on surface currents would provide a more complete picture of wake impacts.

~~Our analysis is based on one complete year of simulations, rather than one season or selected multiday studies, but a~~

495   ~~multiyear study~~ The ocean's response may also mediate these effects of wakes on surface meteorology, as suggested by the simulations of Fischereit et al. (2022b) in the North Sea. Extended simulations, such as those shown here, with a coupled atmosphere-ocean-wave model, could provide more ~~insights into interannual variability.~~ accurate insight into the ocean's role in modulating wake impacts. Such work is ongoing.

Finally, while we focused on one lease area in the northeaster U.S. wind regions, it is important to conduct further analysis on

500   other lease areas in the region and worldwide. Variability in wind patterns, boundary-layer heights, and sea surface temperatures are likely to interact with wind plant wakes in ways that can modify the results presented here.

Code and data availability. The NOW-WAKES simulation data is available at https://dx.doi.org/10.25984/1821404 and code is available at https://zenodo.org/doi/10.5281/zenodo.10993297.
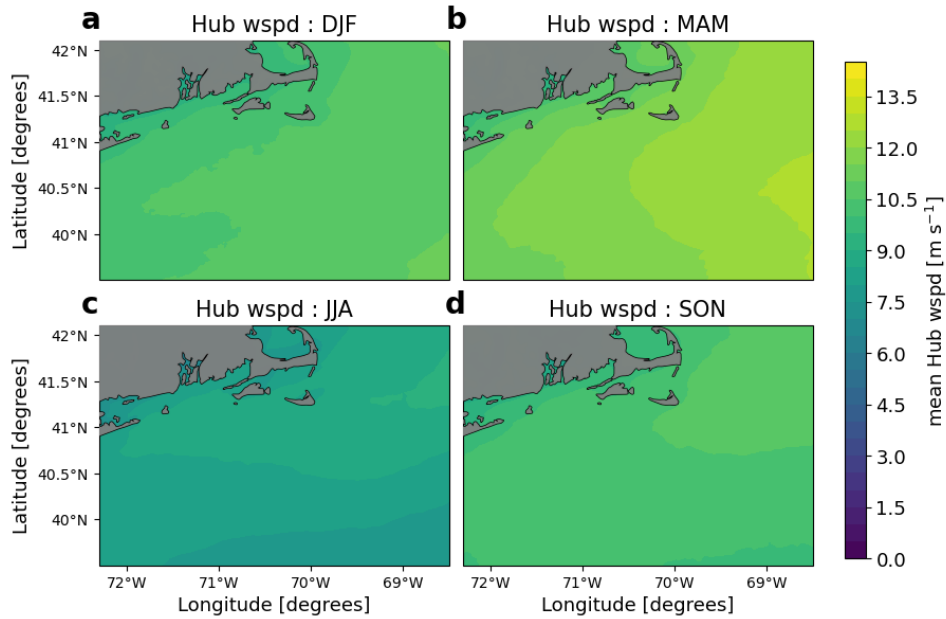
Figure A1. Same as in Fig. 5, but for hub-height wind speed

Appendix A: Additional variable climatologies

A1 Hub-height wind speed climatology

Hub-height wind speeds are fastest during the winter and spring, with means of 10.5 and 11.3 m s^{-1}, respectively (Fig. A1). In the summer and fall, hub-height wind speeds are slightly slower, with means of 7.6 and 9.5 m s^{-1}, respectively. During all seasons, hub-height wind speeds generally increase towards the east.

A2 10 m wind speed climatology

Ten meter wind speeds are fastest during the fall, winter, and spring, with means between 7 and 8 m s^{-1} (Fig. A1). Wind speeds generally increase with distance from the coast during these seasons. In the summer, 10 m wind speeds are slower, with a mean of 5.2 m s^{-1}. A minimum in mean 10 m wind speeds exists to the east of Nantucket in the summer.

A3 2 m temperature climatology

Mean 2 m temperature (T2) is warmest in the summer with a mean of 300 K, and coldest in the winter with a mean of 298 K. T2 is generally warmer to the south of the considered area for all seasons. In the summer, a T2 minimum occurs east of Nantucket. In the winter, minimum temperature occurs close to land. (Fig. A3).
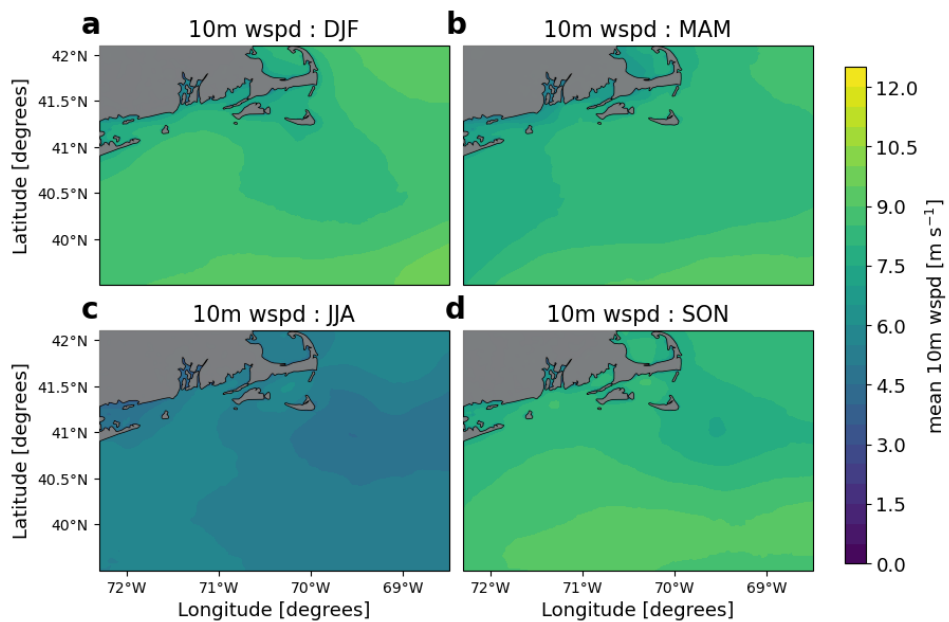
Figure A2. Same as in Fig. 5, but for 10 m wind speed
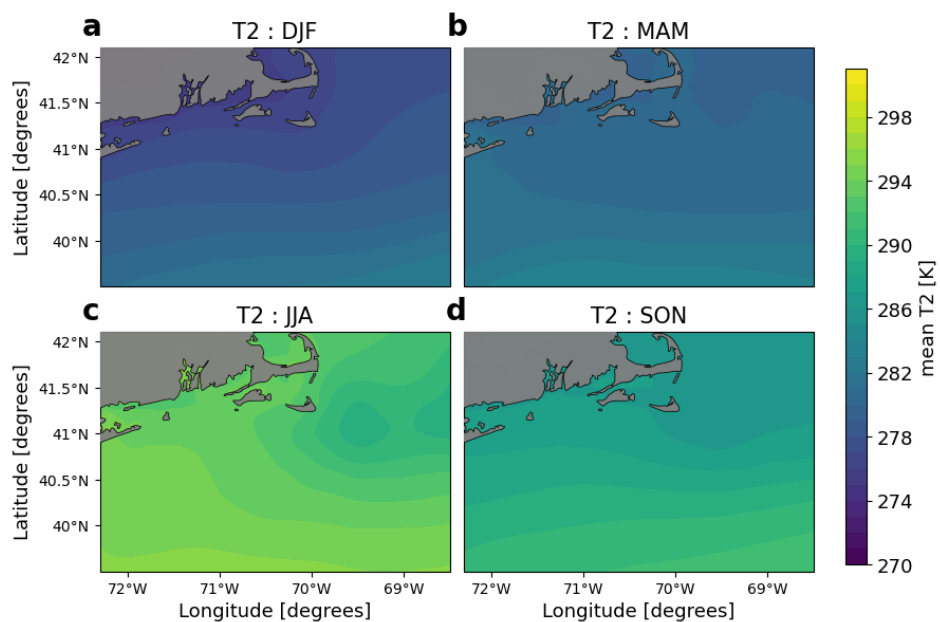
Figure A3. Same as in Fig. 5, but for 2 m temperature.
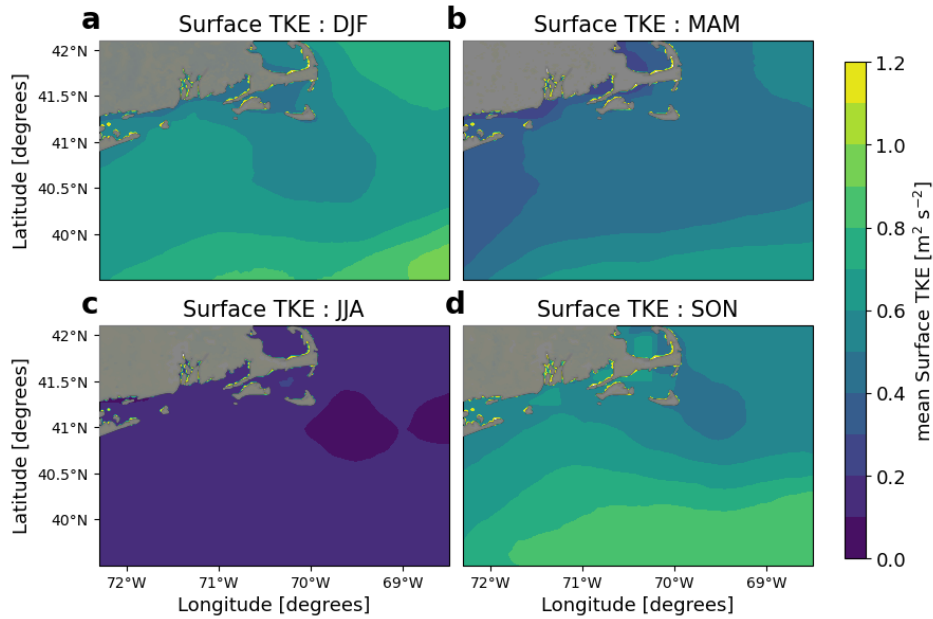
Figure A4. Same as in Fig. 5, but for surface ~~QKE~~ TKE.

A4 Surface ~~QKE~~ TKE climatology

Surface ~~QKE~~ TKE is highest in the fall and winter and smallest in the summer, with mean values of ~~1.5, 1.6, and 0.7~~ 0.75, 0.8, and 0.3 m^2 s^{-2} (Fig. A4). In all seasons, surface ~~QKE~~ TKE is larger to the south, away from the coast. ~~Mean surface QKE is~~

520 ~~similar to values at hub-height that have mean values close to 1 m^2 s^{-2}.~~

A5 Sea surface temperature climatology

Sea surface temperature (SST) is warmest in the summer and coldest in the winter. SST is generally warmer to the south of the considered area for all seasons. In the spring and summer, an SST minimum occurs east of Nantucket. In the winter, minimum SST occurs close to land. (Fig. A5).

525 **Appendix B: Meteorological impacts of wind plant wakes when turbine thrust coefficient becomes small**

As seen in Figure 9, the largest hub-height wind speed deficits occur for winds faster than 11 m s^{-1}. However, when winds faster than 15 m s^{-1} are partitioned out (Figure B1f), the wind speed deficit is smaller due to the very reduced thrust coefficient (Figure 2b).

In contrast, when wind speeds increase past 15 m s^{-1}, the effects on 10 m winds continue to grow, with larger accelerations

530 near the surface (Figure B2f) in faster winds than in moderate winds (Figure B2e).,
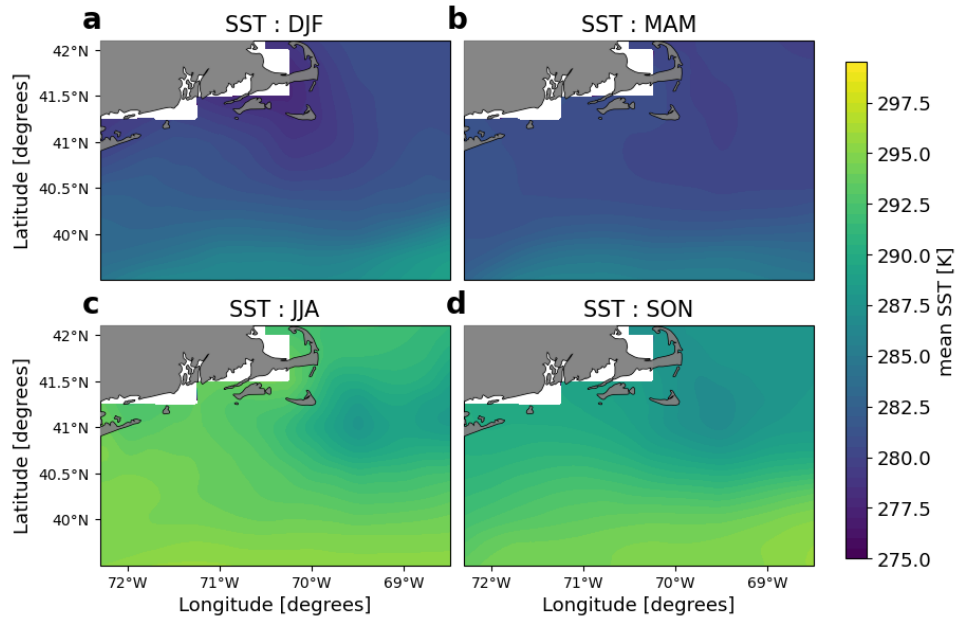
Figure A5. Same as in Fig. 5, but for SST.

Appendix C: Meteorological impacts of wind plant wakes as a function of wind direction

Meteorological impacts of offshore wind farms also vary with wind direction. These results are likely driven by effects of atmospheric stability, as each stability class is associated with a dominant range of wind directions (Fig. 6). In particular, southwesterly winds almost always occur during stable conditions.

535 ### C1   Wind plant wake impacts on hub-height wind speed

All wind directions observe a wind speed deficit both within and downwind of the wind plant (Fig. C1). Southwesterly winds have the strongest wind speed deficit within the wind plant and a larger wake than the other wind directions. In fact, southwesterly winds are typically associated with stable conditions, which are associated with larger wakes.

C2   Wind plant wake impacts on boundary layer height

540 In the vicinity of wind plants, the PBLH increases for all wind directions (Figure C2). This effect is the strongest when there is southwesterly flow (i.e., stable conditions) and weaker for the other three quadrants. Southwesterly and northeasterly wind both exhibit a downwind reduction in PBL, while this effect is minimal for southeasterly winds and nonexistent for northwesterly winds. The downwind reduction in PBLH is strongest for southwesterly winds.
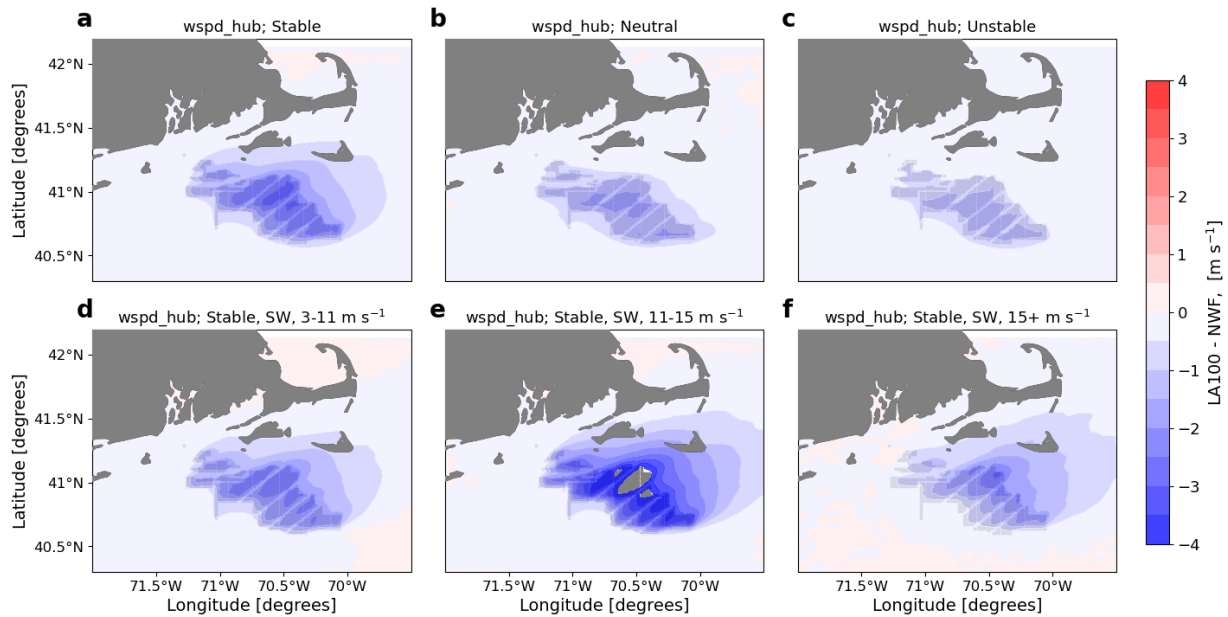
Figure B1. Mean hub-height wind speed difference between the LA100 and NWF simulations in (a) stable conditions, (b) neutral conditions, (c) unstable conditions, (d) 3-11 m s^{-1}, (e) 11-15 m s^{-1}, and (f) 15+ m s^{-1}. Panels d, e, and f are only during times with southwesterly winds. Turbines are marked in gray. Compare to Figure 9.

C3   Wind plant wake impacts on 2-m temperature

545 The largest temperature differences occur during southwesterly flow (Figure C3). Temperatures increase by around 0.1 degrees Celsius in the lease area, and decrease by a similar amount downwind of the wind plant. Temperature differences are much smaller for other wind directions. In general, southerly winds are associated with an increase in temperature within the wind plant and a reduction in temperature outside of the wind plant. Temperature differences are very small for northerly winds. When winds are from the northeast, a slight warming is observed downwind of the wind plant.

550 ## C4   Wind plant wake impacts on surface sensible heat flux

Heat fluxes are reduced within the wind plant for all wind directions (Fig. C4). The strongest reduction in heat flux occurs for northwesterly winds, with reductions of up to 3 W m^{-2}. The other 3 quadrants see differences of around 2 W m^{-2} within the wind plant. When winds are northerly, heat flux is also reduced downwind of the wind plant, with the magnitude decreasing with distance from the wind plant. In contrast, heat flux increases downwind of the wind plant when winds are from
555 the southwest. In addition, heat flux is slightly elevated in the immediate upwind direction.
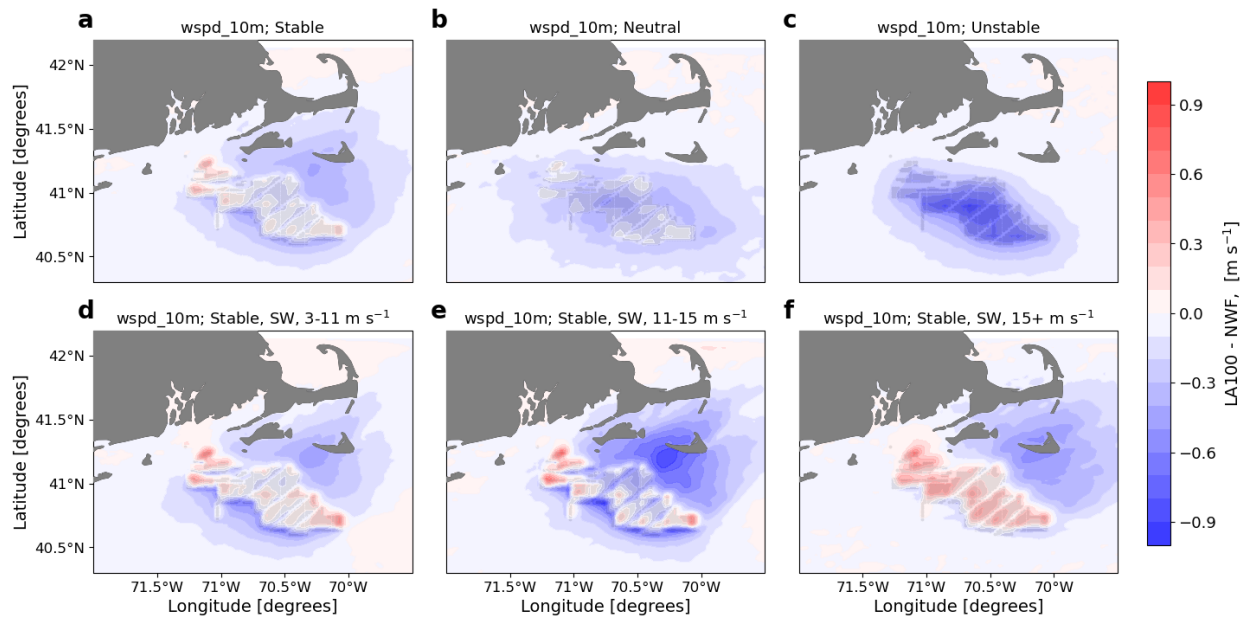
Figure B2. Mean 10 m wind speed difference between the LA100 and NWF simulations in (a) stable conditions, (b) neutral conditions, (c) unstable conditions, (d) 3-11 m s^{-1}, (e) 11-15 m s^{-1}, and (f) 15+ m s^{-1}. Panels d, e, and f are only during times with southwesterly winds. Turbines are marked in gray. Compare to Figure 10.

C5 Wind plant wake impacts on hub-height ~~QKE~~TKE

Hub-height ~~QKE~~ TKE increases similarly for all wind directions (Fig. C5).

C6 Wind plant wake impacts on surface ~~QKE~~TKE

Surface ~~QKE~~ TKE increases within the wind lease area for all wind directions (Fig. C6). Surface ~~QKE~~ TKE increases more when winds are from the northwest or the northeast, with values over 0.3 J kg $^{-1}$. Southerly winds are associated with an increase in ~~QKE~~ TKE closer to 0.2 J kg $^{-1}$. We also notice a downwind reduction in surface ~~QKE~~ TKE for all wind directions, although the magnitude of the reduction is larger for northerly winds.

Author contributions. JKL and NB conceptualized the project and acquired funding and resources for the project. DR completed the WRF simulations and provided the dataset. DQ carried out the formal analysis and investigation, including developing software and carrying out the visualization, with supervision from JKL and NB. DQ prepared the initial draft. All authors reviewed and edited the publication.

Competing interests. At least one of the (co-)authors is a member of the editorial board of Wind Energy Science.
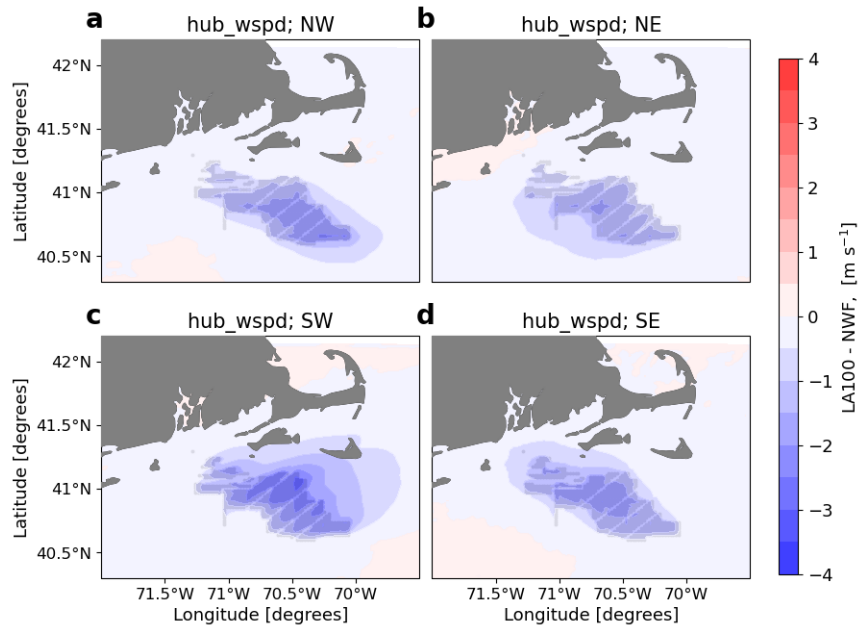
Figure C1. Mean hub-height wind speed difference between the LA100 and NWF simulations for (a) NE, (b) NW, (c) SE, and (d) SW wind directions. Turbines are marked in gray.

Acknowledgements. This research was performed using computational resources sponsored by the U.S. Department of Energy's Office of Energy Efficiency and Renewable Energy and located at the National Renewable Energy Laboratory. This work was supported in part by the U.S. Department of Energy, Office of Science, Office of Workforce Development for Teachers and Scientists under the Science Undergraduate Laboratory Internship program.

570
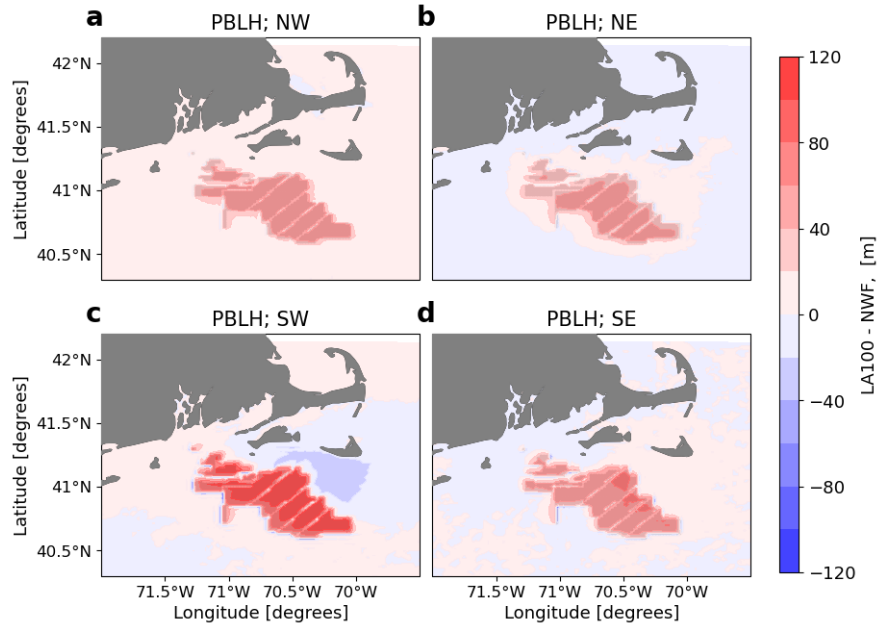
Figure C2. Mean PBLH difference between the LA100 and NWF simulations for (a) NE, (b) NW, (c) SE, and (d) SW wind directions. Turbines are marked in gray.
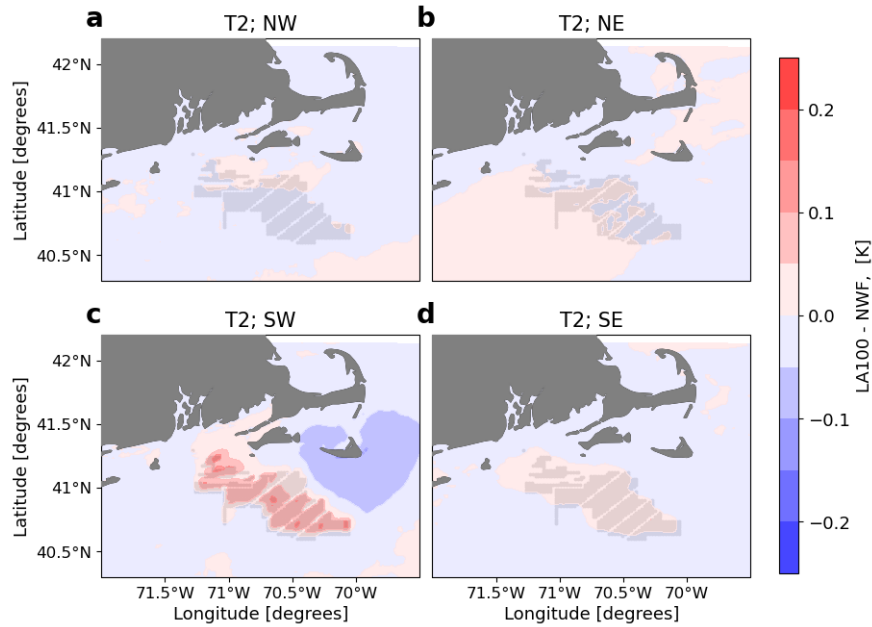
Figure C3. Mean 2-m temperature difference between the LA100 and NWF simulations for (a) NE, (b) NW, (c) SE, and (d) SW wind directions. Turbines are marked in gray.
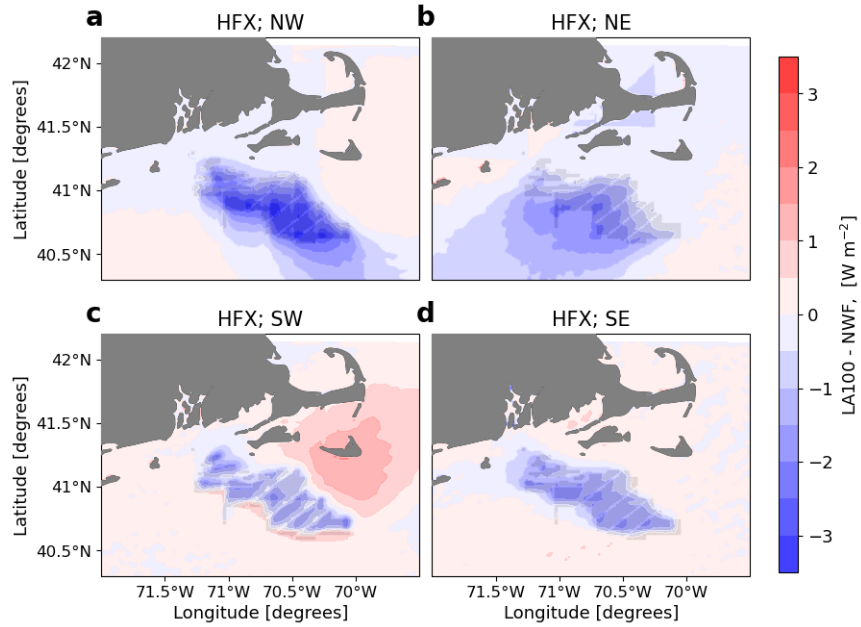
Figure C4. Mean heat flux difference between the LA100 and NWF simulations for (a) NE, (b) NW, (c) SE, and (d) SW wind directions. Turbines are marked in gray.
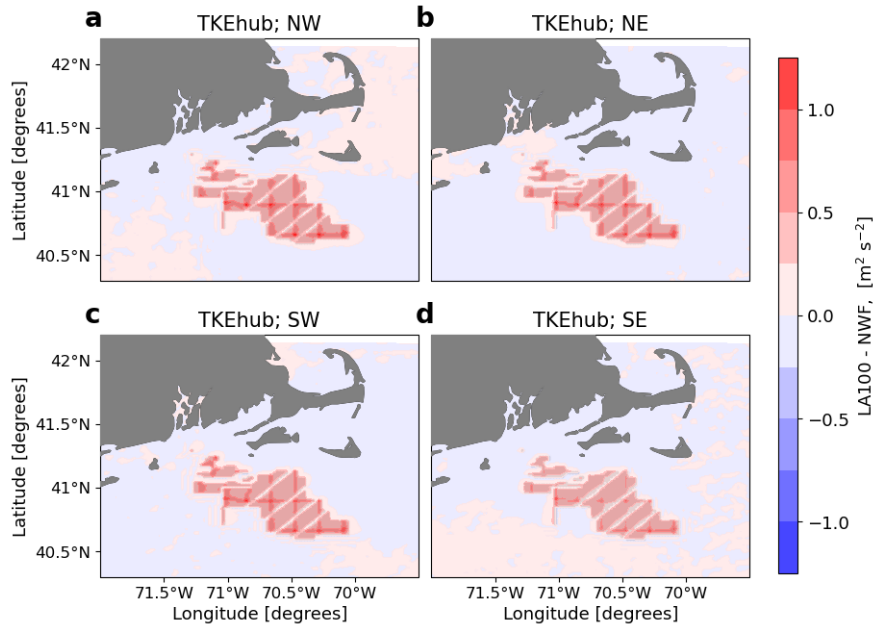
Figure C5. Mean hub-height ~~QKE~~ TKE difference between the LA100 and NWF simulations for (a) NE, (b) NW, (c) SE, and (d) SW wind directions. Turbines are marked in gray.
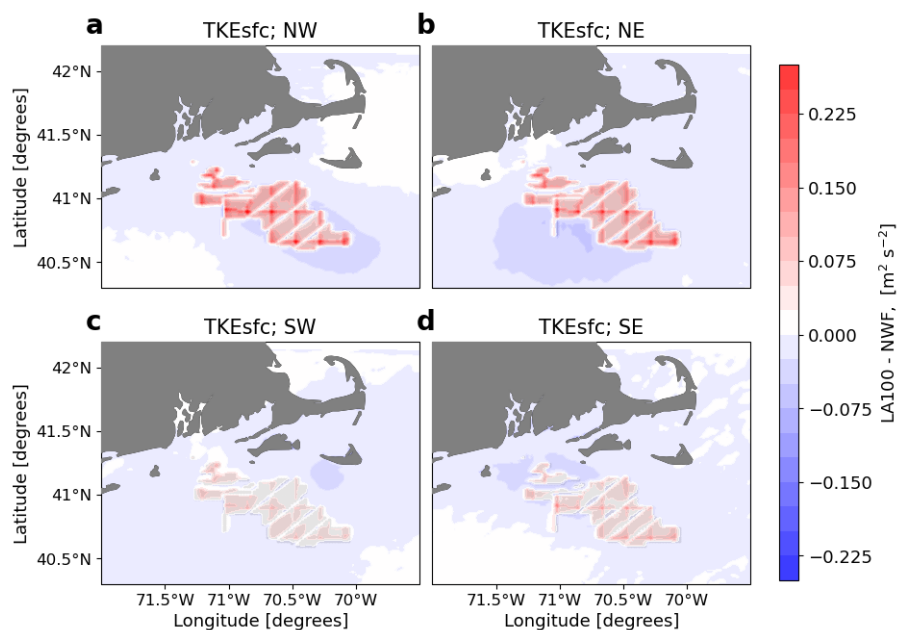
Figure C6. Mean surface ~~QKE~~ TKE difference between the LA100 and NWF simulations for (a) NE, (b) NW, (c) SE, and (d) SW wind directions. Turbines are marked in gray.

References

Abkar, M. and Porté-Agel, F.: The Effect of Free-Atmosphere Stratification on Boundary-Layer Flow and Power Output from Very Large Wind Farms, Energies, 6, 2338–2361, https://doi.org/10.3390/en6052338, number: 5 Publisher: Multidisciplinary Digital Publishing Institute, 2013.

Ali, K., Schultz, D. M., Revell, A., Stallard, T., and Ouro, P.: Assessment of Five Wind-Farm Parameterizations in the Weather Research and Forecasting Model: A Case Study of Wind Farms in the North Sea, Monthly Weather Review, 151, 2333–2359, https://doi.org/10.1175/MWR-D-23-0006.1, publisher: American Meteorological Society Section: Monthly Weather Review, 2023.

Ancell, B. C., Bogusz, A., Lauridsen, M. J., and Nauert, C. J.: Seeding Chaos: The Dire Consequences of Numerical Noise in NWP Perturbation Experiments, Bulletin of the American Meteorological Society, 99, 615–628, https://doi.org/10.1175/BAMS-D-17-0129.1, 2018.

Archer, C. L., Wu, S., Vasel-Be-Hagh, A., Brodie, J. F., Delgado, R., St. Pé, A., Oncley, S., and Semmer, S.: The VERTEX field campaign: observations of near-ground effects of wind turbine wakes, Journal of Turbulence, 20, 64–92, https://doi.org/10.1080/14685248.2019.1572161, publisher: Taylor & Francis _eprint: https://doi.org/10.1080/14685248.2019.1572161, 2019.

Archer, C. L., Wu, S., Ma, Y., and Jiménez, P. A.: Two Corrections for Turbulent Kinetic Energy Generated by Wind Farms in the WRF Model, Monthly Weather Review, 148, 4823 – 4835, https://doi.org/10.1175/MWR-D-20-0097.1, 2020.

Armstrong, A., Burton, R. R., Lee, S. E., Mobbs, S., Ostle, N., Smith, V., Waldron, S., and Whitaker, J.: Ground-level climate at a peatland wind farm in Scotland is affected by wind turbine operation, Environmental Research Letters, 11, 044 024, https://doi.org/10.1088/1748-9326/11/4/044024, publisher: IOP Publishing, 2016.

Baidya Roy, S. and Traiteur, J. J.: Impacts of wind farms on surface air temperatures, Proceedings of the National Academy of Sciences, 107, 17 899–17 904, https://doi.org/10.1073/pnas.1000493107, publisher: National Academy of Sciences Section: Physical Sciences, 2010.

Bodini, N., Lundquist, J. K., Zardi, D., and Handschy, M.: Year-to-year correlation, record length, and overconfidence in wind resource assessment, Wind Energy Science, 1, 115–128, https://doi.org/10.5194/wes-1-115-2016, 2016.

Bodini, N., Lundquist, J. K., and Moriarty, P.: Wind plants can impact long-term local atmospheric conditions, Scientific Reports, 11, 22 939, https://doi.org/10.1038/s41598-021-02089-2, number: 1 Publisher: Nature Publishing Group, 2021.

Bodini, N., Optis, M., Liu, Y., Gaudet, B., Krishnamurthy, R., Kumler, A., Rosencrans, D., Rybchuk, A., Tai, S.-L., Berg, L., Musial, W., Lundquist, J., Purkayastha, A., Young, E., and Draxl, C.: Causes of and Solutions to Wind Speed Bias in NREL's 2020 Offshore Wind Resource Assessment for the California Pacific Outer Continental Shelf, Tech. Rep. NREL/TP–5000-88215, 2318705, MainId:88990, https://doi.org/10.2172/2318705, 2024a.

Bodini, N., Optis, M., Redfern, S., Rosencrans, D., Rybchuk, A., Lundquist, J. K., Pronk, V., Castagneri, S., Purkayastha, A., Draxl, C., Krishnamurthy, R., Young, E., Roberts, B., Rosenlieb, E., and Musial, W.: The 2023 National Offshore Wind data set (NOW-23), Earth System Science Data, 16, 1965–2006, https://doi.org/10.5194/essd-16-1965-2024, publisher: Copernicus GmbH, 2024b.

Bureau of Ocean Energy Management: Offshore Renewable Activities | Bureau of Ocean Energy Management — boem.gov, https://www.boem.gov/renewable-energy/offshore-renewable-activities, 2023.

Chang, R., Zhu, R., and Guo, P.: A Case Study of Land-Surface-Temperature Impact from Large-Scale Deployment of Wind Farms in China from Guazhou, Remote Sensing, 8, 790, https://doi.org/10.3390/rs8100790, number: 10 Publisher: Multidisciplinary Digital Publishing Institute, 2016.

Christiansen, M. B. and Hasager, C. B.: Wake effects of large offshore wind farms identified from satellite SAR, Remote Sensing of Environment, 98, 251–268, https://doi.org/https://doi.org/10.1016/j.rse.2005.07.009, 2005.

Daewel, U., Akhtar, N., Christiansen, N., and Schrum, C.: Offshore wind farms are projected to impact primary production and bottom water deoxygenation in the North Sea, Communications Earth & Environment, 3, 1–8, https://doi.org/10.1038/s43247-022-00625-0, number: 1 Publisher: Nature Publishing Group, 2022.

Draxl, C., Hahmann, A. N., Peña, A., and Giebel, G.: Evaluating winds and vertical wind shear from Weather Research and Forecasting model forecasts using seven planetary boundary layer schemes, Wind Energy, 17, 39–55, https://doi.org/10.1002/we.1555, _eprint: https://onlinelibrary.wiley.com/doi/pdf/10.1002/we.1555, 2014.

Dörenkämper, M., Witha, B., Steinfeld, G., Heinemann, D., and Kühn, M.: The impact of stable atmospheric boundary layers on wind-turbine wakes within offshore wind farms, Journal of Wind Engineering and Industrial Aerodynamics, 144, 146–153, https://doi.org/10.1016/j.jweia.2014.12.011, 2015.

Ester, M., Kriegel, H.-P., Sander, J., and Xu, X.: A density-based algorithm for discovering clusters in large spatial databases with noise, in: Proceedings of the Second International Conference on Knowledge Discovery and Data Mining, KDD'96, p. 226–231, AAAI Press, 1996.

Fischereit, J., Brown, R., Larsén, X. G., Badger, J., and Hawkes, G.: Review of Mesoscale Wind-Farm Parametrizations and Their Applications, Boundary-Layer Meteorology, 182, 175–224, https://doi.org/10.1007/s10546-021-00652-y, 2022a.

Fischereit, J., Larsén, X. G., and Hahmann, A. N.: Climatic Impacts of Wind-Wave-Wake Interactions in Offshore Wind Farms, Frontiers in Energy Research, 10, https://doi.org/10.3389/fenrg.2022.881459, publisher: Frontiers, 2022b.

Fitch, A. C., Olson, J. B., Lundquist, J. K., Dudhia, J., Gupta, A. K., Michalakes, J., and Barstad, I.: Local and Mesoscale Impacts of Wind Farms as Parameterized in a Mesoscale NWP Model, Monthly Weather Review, 140, 3017 – 3038, https://doi.org/https://doi.org/10.1175/MWR-D-11-00352.1, 2012.

Fitch, A. C., Lundquist, J. K., and Olson, J. B.: Mesoscale Influences of Wind Farms throughout a Diurnal Cycle, Monthly Weather Review, 141, 2173 – 2198, https://doi.org/10.1175/MWR-D-12-00185.1, 2013.

Gadde, S. N. and Stevens, R. J. A. M.: Interaction between low-level jets and wind farms in a stable atmospheric boundary layer, Phys. Rev. Fluids, 6, 014 603, https://doi.org/10.1103/PhysRevFluids.6.014603, 2021.

Golbazi, M., Archer, C. L., and Alessandrini, S.: Surface impacts of large offshore wind farms, Environmental Research Letters, 17, 064 021, https://doi.org/10.1088/1748-9326/ac6e49, publisher: IOP Publishing, 2022.

Gryning, S.-E., Batchvarova, E., Br√°mmer, B., J√∏rgensen, H., and Larsen, S.: On the extension of the wind profile over homogeneous terrain beyond the surface boundary layer, Boundary-Layer Meteorology, 124, 251–268, https://doi.org/10.1007/s10546-007-9166-9, 2007.

Harris, R., Zhou, L., and Xia, G.: Satellite Observations of Wind Farm Impacts on Nocturnal Land Surface Temperature in Iowa, Remote Sensing, 6, 12 234–12 246, https://doi.org/10.3390/rs61212234, 2014.

Juliano, T. W., Kosović, B., Jiménez, P. A., Eghdami, M., Haupt, S. E., and Martilli, A.: "Gray Zone" Simulations using a Three-Dimensional Planetary Boundary Layer Parameterization in the Weather Research and Forecasting Model, Monthly Weather Review, -1, https://doi.org/10.1175/MWR-D-21-0164.1, publisher: American Meteorological Society Section: Monthly Weather Review, 2021.

Kosović, B., Jimenez Munoz, P., Juliano, T. W., Martilli, A., Eghdami, M., Barros, A. P., and Haupt, S. E.: Three-Dimensional Planetary Boundary Layer Parameterization for High-Resolution Mesoscale Simulations, Journal of Physics: Conference Series, 1452, 012 080, https://doi.org/10.1088/1742-6596/1452/1/012080, 2020.

Larsén, X. G. and Fischereit, J.: A case study of wind farm effects using two wake parameterizations in the Weather Research and Forecasting (WRF) model (V3.7.1) in the presence of low-level jets, Geoscientific Model Development, 14, 3141–3158, https://doi.org/10.5194/gmd-14-3141-2021, publisher: Copernicus GmbH, 2021.

Lauridsen, M. J. and Ancell, B. C.: Nonlocal Inadvertent Weather Modification Associated with Wind Farms in the Central United States, https://doi.org/https://doi.org/10.1155/2018/2469683, iSSN: 1687-9309 Pages: e2469683 Publisher: Hindawi Volume: 2018, 2018.

Lee, J. C. Y. and Lundquist, J. K.: Evaluation of the wind farm parameterization in the Weather Research and Forecasting model (version 3.8.1) with meteorological and turbine power data, Geosci. Model Dev., 10, 4229–4244, https://doi.org/10.5194/gmd-10-4229-2017, 2017.

Liu, K., Du, J., Larsén, X. G., and Lian, Z.: Spatiotemporal Variations of Ocean Upwelling and Downwelling Induced by Wind Wakes of Offshore Wind Farms, Journal of Marine Science and Engineering, 11, 2020, https://doi.org/10.3390/jmse11102020, number: 10 Publisher: Multidisciplinary Digital Publishing Institute, 2023.

Liu, Y., Gaudet, B., Krishnamurthy, R., Tai, S.-L., Berg, L. K., Bodini, N., Rybchuk, A., and Kumler, A.: Identifying Meteorological Drivers for Errors in Modeled Winds along the Northern California Coast, Monthly Weather Review, 152, 455–469, https://doi.org/10.1175/MWR-D-23-0030.1, publisher: American Meteorological Society Section: Monthly Weather Review, 2024.

Lu, H. and Porté-Agel, F.: Large-eddy simulation of a very large wind farm in a stable atmospheric boundary layer, Physics of Fluids, 23, 065 101, https://doi.org/10.1063/1.3589857, 2011.

Lundquist, J. K., DuVivier, K. K., Kaffine, D., and Tomaszewski, J. M.: Costs and consequences of wind turbine wake effects arising from uncoordinated wind energy development, Nature Energy, 4, 26–34, https://doi.org/10.1038/s41560-018-0281-2, 2019.

Luo, L., Zhuang, Y., Duan, Q., Dong, L., Yu, Y., Liu, Y., Chen, K., and Gao, X.: Local climatic and environmental effects of an onshore wind farm in North China, Agricultural and Forest Meteorology, 308-309, 108 607, https://doi.org/10.1016/j.agrformet.2021.108607, 2021.

Maas, O. and Raasch, S.: Wake properties and power output of very large wind farms for different meteorological conditions and turbine spacings: a large-eddy simulation case study for the German Bight, Wind Energy Science, 7, 715–739, https://doi.org/10.5194/wes-7-715-2022, publisher: Copernicus GmbH, 2022.

Moriarty, P. J., Bodini, N., Letizia, S., Abraham, A., ashley, t., Bärfuss, K., Barthelmie, R. J., Brewer, A., Brugger, P., Feuerle, T., Frère, A., Goldberger, L., Gottschall, J., Hamilton, N., Herges, T., Hirth, B., Hung, L.-Y. L., Iungo, G. V., Ivanov, H., Kaul, C. M., Kern, S., Klein, P., Krishnamurthy, R., Lampert, A., Lundquist, J. K., Morris, V. R., Newsom, R., Pekour, M., Pichugina, Y., Porté-Agel, F., Pryor, S. C., Scholbrock, A., Schroeder, J., Shartzer, s., Simley, E., Vöhringer, L., Wharton, S., and Zalkind, D.: Overview of Preparation for the American Wake Experiment (AWAKEN), Journal of Renewable and Sustainable Energy, accepted for publication, 2024.

Nakanishi, M. and Niino, H.: Development of an Improved Turbulence Closure Model for the Atmospheric Boundary Layer, Journal of the Meteorological Society of Japan. Ser. II, 87, 895–912, https://doi.org/10.2151/jmsj.87.895, 2009.

Nielsen-Gammon, J. W., Powell, C. L., Mahoney, M. J., Angevine, W. M., Senff, C., White, A., Berkowitz, C., Doran, C., and Knupp, K.: Multisensor Estimation of Mixing Heights over a Coastal City, Journal of Applied Meteorology and Climatology, 47, 27 – 43, https://doi.org/10.1175/2007JAMC1503.1, 2008.

Olson, J. B., Kenyon, J. S., Angevine, W. M., Brown, J. M., Pagowski, M., and Sušelj, K.: A Description of the MYNN-EDMF Scheme and the Coupling to Other Components in WRF–ARW, Tech. Rep. OAR GSD-61, NOAA, https://repository.library.noaa.gov/view/noaa/19837, publisher: Earth System Research Laboratory (U.S.), Global Systems Division, 2019.

680   Peña, A., Mirocha, J. D., and Laan, M. P. v. d.: Evaluation of the Fitch Wind-Farm Wake Parameterization with Large-Eddy Simulations of Wakes Using the Weather Research and Forecasting Model, Monthly Weather Review, 150, 3051–3064, https://doi.org/10.1175/MWR-D-22-0118.1, publisher: American Meteorological Society Section: Monthly Weather Review, 2022.

Platis, A., Siedersleben, S. K., Bange, J., Lampert, A., Bärfuss, K., Hankers, R., Cañadillas, B., Foreman, R., Schulz-Stellenfleth, J., Djath, B., Neumann, T., and Emeis, S.: First in situ evidence of wakes in the far field behind offshore wind farms, Scientific Reports, 8,

685   https://doi.org/10.1038/s41598-018-20389-y, 2018.

Platis, A., Bange, J., Bärfuss, K., Canadillas, B., Hundhausen, M., Djath, B., Lampert, A., Schulz-Stellenfleth, J., Siedersleben, S., Neumann, T., and Emeis, S.: Long-range modifications of the wind field by offshore wind parks – results of the project WIPAFF, Meteorologische Zeitschrift, 29, 355 – 376, https://doi.org/10.1127/metz/2020/1023, 2020.

Pryor, S. C. and Barthelmie, R. J.: Wind shadows impact planning of large offshore wind farms, Applied Energy, 359, 122 755,

690   https://doi.org/https://doi.org/10.1016/j.apenergy.2024.122755, 2024.

Pryor, S. C., Barthelmie, R. J., and Shepherd, T. J.: Wind power production from very large offshore wind farms, Joule, 5, 2663–2686, https://doi.org/10.1016/j.joule.2021.09.002, 2021.

Raghukumar, K., Chartrand, C., Chang, G., Cheung, L., and Roberts, J.: Effect of Floating Offshore Wind Turbines on Atmospheric Circulation in California, Frontiers in Energy Research, 10, https://doi.org/10.3389/fenrg.2022.863995, publisher: Frontiers, 2022.

695   Raghukumar, K., Nelson, T., Jacox, M., Chartrand, C., Fiechter, J., Chang, G., Cheung, L., and Roberts, J.: Projected cross-shore changes in upwelling induced by offshore wind farm development along the California coast, Communications Earth & Environment, 4, 1–12, https://doi.org/10.1038/s43247-023-00780-y, publisher: Nature Publishing Group, 2023.

Rajewski, D. A., Takle, E. S., Lundquist, J. K., Oncley, S., Prueger, J. H., Horst, T. W., Rhodes, M. E., Pfeiffer, R., Hatfield, J. L., Spoth, K. K., and Doorenbos, R. K.: Crop Wind Energy Experiment (CWEX): Observations of Surface-Layer, Boundary Layer, and Mesoscale

700   Interactions with a Wind Farm, Bulletin of the American Meteorological Society, 94, 655–672, https://doi.org/10.1175/BAMS-D-11-00240.1, 2013.

Rajewski, D. A., Takle, E. S., Lundquist, J. K., Prueger, J. H., Pfeiffer, R. L., Hatfield, J. L., Spoth, K. K., and Doorenbos, R. K.: Changes in fluxes of heat, H2O, and CO2 caused by a large wind farm, Agricultural and Forest Meteorology, 194, 175–187, https://doi.org/10.1016/j.agrformet.2014.03.023, 2014.

705   Redfern, S., Optis, M., Xia, G., and Draxl, C.: Offshore wind energy forecasting sensitivity to sea surface temperature input in the Mid-Atlantic, Wind Energy Science, 8, 1–23, https://doi.org/10.5194/wes-8-1-2023, publisher: Copernicus GmbH, 2023.

Rhodes, M. E. and Lundquist, J. K.: The Effect of Wind-Turbine Wakes on Summertime US Midwest Atmospheric Wind Profiles as Observed with Ground-Based Doppler Lidar, Boundary-Layer Meteorology, 149, 85–103, https://doi.org/10.1007/s10546-013-9834-x, 2013.

Rosencrans, D., Lundquist, J. K., Optis, M., Rybchuk, A., Bodini, N., and Rossol, M.: Seasonal variability of wake impacts on US mid-

710   Atlantic offshore wind plant power production, Wind Energy Science, 9, 555–583, https://doi.org/10.5194/wes-9-555-2024, publisher: Copernicus GmbH, 2024.

Rybchuk, A., Juliano, T. W., Lundquist, J. K., Rosencrans, D., Bodini, N., and Optis, M.: The sensitivity of the fitch wind farm parameterization to a three-dimensional planetary boundary layer scheme, Wind Energy Science, 7, 2085–2098, https://doi.org/10.5194/wes-7-2085-2022, publisher: Copernicus GmbH, 2022.

715   Sathe, A., Gryning, S.-E., and Peña, A.: Comparison of the atmospheric stability and wind profiles at two wind farm sites over a long marine fetch in the North Sea, Wind Energy, 14, 767–780, https://doi.org/10.1002/we.456, 2011.

Siedersleben, S. K., Lundquist, J. K., Platis, A., Bange, J., Bärfuss, K., Lampert, A., Cañadillas, B., Neumann, T., and Emeis, S.: Micrometeorological impacts of offshore wind farms as seen in observations and simulations, Environmental Research Letters, 13, 124 012, https://doi.org/10.1088/1748-9326/aaea0b, 2018a.

Siedersleben, S. K., Platis, A., Lundquist, J. K., Lampert, A., Bärfuss, K., Cañadillas, B., Djath, B., Schulz-Stellenfleth, J., Bange, J., Neumann, T., and Emeis, S.: Evaluation of a Wind Farm Parametrization for Mesoscale Atmospheric Flow Models with Aircraft Measurements, Meteorologische Zeitschrift, 27, 401–415, https://doi.org/10.1127/metz/2018/0900, 2018b.

Siedersleben, S. K., Platis, A., Lundquist, J. K., Djath, B., Lampert, A., Bärfuss, K., Cañadillas, B., Schulz-Stellenfleth, J., Bange, J., Neumann, T., and Emeis, S.: Turbulent kinetic energy over large offshore wind farms observed and simulated by the mesoscale model WRF (3.8.1), Geoscientific Model Development, 13, 249–268, https://doi.org/10.5194/gmd-13-249-2020, publisher: Copernicus GmbH, 2020.

Skamarock, C., Klemp, B., Dudhia, J., Gill, O., Liu, Z., Berner, J., Wang, W., Powers, G., Duda, G., Barker, D., and Huang, X.-y.: A Description of the Advanced Research WRF Model Version 4.3, Tech. Rep. NCAR/TN-556+STR, https://opensky.ucar.edu/islandora/object/technotes%3A588/, 2021.

Slawsky, L. M., Zhou, L., Roy, S. B., Xia, G., Vuille, M., and Harris, R. A.: Observed Thermal Impacts of Wind Farms Over Northern Illinois, Sensors, 15, 14 981–15 005, https://doi.org/10.3390/s150714981, number: 7 Publisher: Multidisciplinary Digital Publishing Institute, 2015.

Smith, C. M., Barthelmie, R. J., and Pryor, S. C.: *In situ* observations of the influence of a large onshore wind farm on near-surface temperature, turbulence intensity and wind speed profiles, Environmental Research Letters, 8, 034 006, https://doi.org/10.1088/1748-9326/8/3/034006, 2013.

Stull, R. B., ed.: An Introduction to Boundary Layer Meteorology, Springer Netherlands, Dordrecht, https://doi.org/10.1007/978-94-009-3027-8, 1988.

U.S. Department of Energy: DOE Releases Strategy to Accelerate and Expand Domestic Offshore Wind Deployment, https://www.energy.gov/articles/doe-releases-strategy-accelerate-and-expand-domestic-offshore-wind-deployment, 2023.

Vanderwende, B. J., Kosović, B., Lundquist, J. K., and Mirocha, J. D.: Simulating effects of a wind-turbine array using LES and RANS, Journal of Advances in Modeling Earth Systems, 8, 1376–1390, https://doi.org/10.1002/2016MS000652, 2016.

Walsh-Thomas, J. M., Cervone, G., Agouris, P., and Manca, G.: Further evidence of impacts of large-scale wind farms on land surface temperature, Renewable and Sustainable Energy Reviews, 16, 6432–6437, https://doi.org/10.1016/j.rser.2012.07.004, 2012.

Wu, K. L. and Porté-Agel, F.: Flow Adjustment Inside and Around Large Finite-Size Wind Farms, Energies, 10, https://doi.org/10.3390/en10122164, 2017.

Xia, G., Zhou, L., Freedman, J. M., Roy, S. B., Harris, R. A., and Cervarich, M. C.: A case study of effects of atmospheric boundary layer turbulence, wind speed, and stability on wind farm induced temperature changes using observations from a field campaign, Climate Dynamics, 46, 2179–2196, https://doi.org/10.1007/s00382-015-2696-9, 2016.

Xia, G., Zhou, L., Minder, J. R., Fovell, R. G., and Jimenez, P. A.: Simulating impacts of real-world wind farms on land surface temperature using the WRF model: physical mechanisms, Climate Dynamics, 53, 1723–1739, https://doi.org/10.1007/s00382-019-04725-0, 2019.

Xia, G., Draxl, C., Optis, M., and Redfern, S.: Detecting and characterizing simulated sea breezes over the US northeastern coast with implications for offshore wind energy, Wind Energy Science, 7, 815–829, https://doi.org/10.5194/wes-7-815-2022, publisher: Copernicus GmbH, 2022.

Zhou, L., Tian, Y., Baidya Roy, S., Dai, Y., and Chen, H.: Diurnal and seasonal variations of wind farm impacts on land surface temperature over western Texas, Climate Dynamics, https://doi.org/10.1007/s00382-012-1485-y, 2012a.

Zhou, L., Tian, Y., Baidya Roy, S., Thorncroft, C., Bosart, L. F., and Hu, Y.: Impacts of wind farms on land surface temperature, Nature Climate Change, 2, 539–543, https://doi.org/10.1038/nclimate1505, number: 7 Publisher: Nature Publishing Group, 2012b.

755